TRANSPORT AND TUNNELING IN MULTIWALLED CARBON NANOTUBES

Reeta Tarkiainen

Dissertation for the degree of Doctor of Science in Technology to be presented with due permission of the Department of Engineering Physics and Mathematics for public examination and debate in Auditorium F1 at Helsinki University of Technology (Espoo, Finland) on the 3rd of June, 2005, at 12 noon.

Helsinki University of Technology
Department of Engineering Physics and Mathematics
Low Temperature Laboratory

Teknillinen korkeakoulu
Teknillisen fysiikan ja matematiikan osasto
Kylmälaboratorio

Distribution:
Helsinki University of Technology
Low Temperature Laboratory
P.O.Box 2200
FI-02015 TKK
Tel. +358-9-451-5795
Fax. +358-9-451-2969
http://boojum.hut.fi/
E-mail: Reeta.Tarkiainen@tkk.fi

This dissertation can be read at http://lib.tkk.fi/Diss/2005/isbn9512277018/

ISBN 951-22-7700-X
ISBN 951-22-7701-8 (pdf)

Otamedia Oy
Espoo 2005

HELSINKI UNIVERSITY OF TECHNOLOGY P.O. BOX 1000, FIN-02015 HUT http://www.hut.fi	ABSTRACT OF DOCTORAL DISSERTATION

Author Reeta Maria Tarkiainen

Name of the dissertation

TRANSPORT AND TUNNELING IN MULTIWALLED CARBON NANOTUBES

Date of manuscript 21.3.2005	Date of the dissertation 3.6.2005
☐ Monograph	☑ Article dissertation (summary + original articles)

Department	Department of Engineering Physics and Mathematics
Laboratory	Low Temperature Laboratory
Field of research	Experimental condensed matter physics
Opponent(s)	Prof. Hélène Bouchiat
Supervisor	Prof. Pekka Hautojärvi
(Instructor)	Prof. Pertti Hakonen

Abstract

Carbon nanotubes are promising new candidates for the construction of molecular-scale electronic circuits. However, the widely varying quality of the material, synthesized using different methods, results in large variation in electronic transport properties. In this Thesis, electronic transport in both disordered and good-quality multiwalled carbon nanotubes was studied. The transport in disordered samples, synthesized using chemical vapor deposition method, was studied to this extent for the first time.

The transport in disordered samples was found to be diffusive. The mean free path is so short that the quantum corrections to conductivity, the weak localization correction and the interaction correction, are best described using the theory for a two-dimensional conductor. The samples are found to be close to the strong localization limit, and the electron dephasing cannot be fully accounted for using the standard electron-electron scattering only. An additional dephasing mechanism is required, such as magnetic impurities. As bias voltage is increased the sample resistance was observed to change in accordance with an electron heating model.

The tunneling conductivity of both disordered and good-quality samples was measured, and a zero bias anomaly was discovered in both cases. However, the results differ due to the larger resistivity of the disordered samples. In the disordered case, the functional form of the anomaly was successfully compared with the non-perturbative theory of electron tunneling into a disordered 1D electrode. In the good-quality samples, the anomaly obeyed a power law, which can result from both environmental quantum fluctuation theory for ultra-small junctions and the Luttinger model. At high voltages the predictions differ, and better agreement with the environmental quantum fluctuation theory was found.

Construction of single-electron transistors, with good charge sensitivity, was demonstrated. Current fluctuations were observed to originate both from background charge fluctuations and resistance fluctuations of the device itself.

Keywords carbon nanotubes, electron transport in mesoscopic systems

UDC	Number of pages 48
ISBN (printed) 951-22-7700-X	ISBN (pdf) 951-22-7701-8
ISBN (others)	ISSN

Publisher Otamedia Oy

Print distribution

☑ The dissertation can be read at http://lib.hut.fi/Diss/ 2005/isbn9512277018/

Acknowledgements

The research presented in this Thesis has been conducted in the Low Temperature Laboratory over a period of six years. I am grateful to the leader of the Low Temperature Laboratory, Prof. Mikko Paalanen for having this opportunity to work there. Besides running the laboratory, he has also found time to take personal interest in the work concerning nanotubes, and has input many valuable ideas. I owe thanks to my instructor Prof. Pertti Hakonen, who has been the main source of ideas regarding this Thesis, and without whose expertise and encouragement this research would have been impossible. He has also shown great patience during the time it has taken to complete this Thesis. I wish to thank my collaborators and co-authors Prof. Markus Ahlskog, Dr. Leif Roschier, and Dr. Jari Penttilä. I have learned a lot from them. The theoretical support of Prof. Edouard Sonin and Dr. Alexander Zyuzin is gratefully acknowledged. I also want to thank the past and present members of the NANO group René Lindell, Mika Sillanpää, Tero Heikkilä, Wu Fan, Taku Tsuneta, Paula Havu, Michel Martin, Antti Paila, Teijo Lehtinen, Julien Delahaye, Takahide Yamaguchi, and Lasse Aaltonen.

I'm grateful to Prof. Christoph Strunk and Doc. Konstantin Arutyunov for the swift pre-examination of the manuscript. I wish to thank Prof. Pekka Hautojärvi for acting as the supervisor of this Thesis on behalf of the Department of Engineering Physics and Mathematics.

I would also like to thank many nice people in and around the LTL, whether permanent or just short-time visitors, Jukka Pekola, Jani Kivioja, Erkki Thuneberg, Juha Tuoriniemi, Wang Taihong, Katsuhiko Inagaki, Antti Finne, Risto Hänninen, Janne Viljas, Juha Kopu, Kirsi Juntunen, Heikki Junes, Antti Kainulainen, Peter Berglund, Jari Kinaret, and Andrei Zaikin. They have been helpful in many ways, from instructive discussions to the invaluable help with various pieces of research equipment. Much appreciated. I would also like to thank the administrative personnel: Marja Holmström, Pirjo Muukkonen, Tuire Koivisto, Liisi Pasanen, Satu Pakarinen, and Teija Halme. The workshop has kindly helped with several small and bigger projects over the years, and I'm grateful to Seppo Kaivola, Juhani Kaasinen,

Markku Korhonen, and the other staff. Also the liquifier personnel deserves thanks for providing the essential liquid helium for the experiments.

I thank my parents Anja and Tapio for being there for me when required, and my husband Antti for providing so much advice, unsolicited or not. Thank you for listening to my sometimes tiresome ramblings, and sharing the highs and lows.

Otaniemi, May 2005

Reeta Tarkiainen

Contents

List of publications

This Thesis is based on the following original publications.

P1 R. Tarkiainen, M. Ahlskog, A. Zyuzin, P. Hakonen, and M. Paalanen, *Transport in strongly disordered multiwalled carbon nanotubes*, Physical Review B **69**, 033402 (2004).

P2 R. Tarkiainen, M. Ahlskog, P. Hakonen, and M. Paalanen, *Transport in disordered carbon nanotubes*, Physica E **18**, 206 (2003).

P3 R. Tarkiainen, M. Ahlskog, P. Hakonen, and M. Paalanen, *Electron heating effects in disordered carbon nanotubes*, In Proceedings of the International Conference on Quantum Transport and Quantum Coherence, Journal of the Physical Society of Japan **72**, Supplement A, 100 (2003).

P4 R. Tarkiainen, M. Ahlskog, M. Paalanen, A. Zyuzin, and P. Hakonen, *Tunneling spectroscopy of disordered multiwalled carbon nanotubes*, Physical Review B **71**, 125425 (2005).

P5 R. Tarkiainen, M. Ahlskog, J. Penttilä, L. Roschier, P. Hakonen, M. Paalanen, and E. Sonin, *Multiwalled carbon nanotube: Luttinger versus Fermi liquid*, Physical Review B **64**, 195412 (2001).

P6 M. Ahlskog, P. Hakonen, M. Paalanen, L. Roschier, and R. Tarkiainen, *Multiwalled carbon nanotubes as building blocks in nanoelectronics*, Journal of Low Temperature Physics **124**, 335 (2001).

P7 M. Ahlskog, R. Tarkiainen, L. Roschier, and P. Hakonen, *Single-electron transistor made of two crossing multiwalled carbon nanotubes and its noise properties*, Applied Physics Letters **77**, 4037 (2000).

P8 L. Roschier, R. Tarkiainen, M. Ahlskog, M. Paalanen, and P. Hakonen, *Multiwalled carbon nanotubes as ultrasensitive electrometers*, Applied Physics Letters **78**, 3295 (2001).

P9 R. Tarkiainen, L. Roschier, M. Ahlskog, M. Paalanen, and P. Hakonen, *Low-frequency current noise and resistance fluctuations in multiwalled carbon nanotubes*, Physica E **28**, 57 (2005).

Author's contribution

The research work described in this Thesis was done in the NANO group of the Low Temperature Laboratory at Helsinki University of Technology. I started working in the NANO group in 1999, at the time when the nanotube transport studies were just started. My first task was to develop sample preparation methods in order to obtain samples with low impedance contacts, mainly using the AFM manipulation. Later on, I was more involved in the measurements, where I have carried the responsibility of the everyday operations, including the refrigeration of the nanotube samples to low temperatures. In the work concerning disordered nanotubes, I was heavily involved in all stages of the work, from planning the experiments and performing the measurements to writing of the final publications.

I have written publications P1-P4 and P9. I did most of the measurements and the data analysis in them as well. I have participated in the preparation of samples for publications P5-P8, and taken part in the measurements and the preparation of the manuscripts for publications P5-P7.

1 Introduction

Carbon is a versatile element which can be found in many forms in nature. A new structural form, carbon nanotube, was discovered in 1991 [1]. Soon after the discovery, it was understood that elemental carbon in this form can conduct electricity very well, and since the nanotubes are also mechanically very robust, they are promising for various electronic applications. Considerable amount of research has been put in the effort to understand the electron transport properties of carbon nanotubes. This Thesis work is a small part of this effort.

The outline of the Thesis is the following. In the introduction, the electronic transport in mesoscopic systems is briefly reviewed from parts which are relevant in what follows (Sec. 1.1). The structure and synthesis of carbon nanotubes are described, and the electronic transport in them, according to the present understanding, is reviewed (Sec. 1.2). In Ch. 2 the experimental techniques used in this work are described. In Ch. 3 the transport measurements on disordered carbon nanotubes are discussed, and Ch. 4 is about tunneling experiments on nanotubes. The tunneling conductivity of both disordered and good-quality nanotubes has been studied. In Ch. 5 the possibility of using nanotubes for single electronics is discussed, and finally in Ch. 6 conclusions are given.

1.1 Electronic transport in mesoscopic systems

As the size of a conductor is decreased, Ohm's law is no longer strictly valid and size-dependent phenomena arise. In this section these phenomena and the different relevant length scales will be introduced. Complete discussion can be found e. g. in Ref. [2].

The electron mean free path L_{m} determines the transport regime: if L_{m} is longer than the sample length L, the electrons are ballistic. In the other limit the transport can be classified either as diffusive or classical, depending

on whether elastic or inelastic scattering processes contribute more to $L_{\rm m}$. Unlike a superconductor, a ballistic wire has a non-zero resistance. As the transverse size of the wire decreases, the spacing of the states increases and the continuum approximation breaks down. Due to the finite number of transverse modes available, the conductance is quantized, and is given by $G = Me^2/h$, where M is the number of modes.

In the diffusive regime, the elastic scattering is much more common than inelastic scattering, which destroys the phase coherence of the electrons. The interference effects between electron waves become important, giving rise to effects such as weak localization magnetoresistance, universal conductance fluctuations and Aharonov-Bohm (A-B) effect (see, e. g. [3, 4]). Localization arises due to the interference between time reversed electron waves, traversing a closed loop in opposite directions. Typically the interference is constructive, and enhances backscattering (destructive interference can arise due to strong spin-orbit scattering, and is referred to as anti-localization). For this effect to be observable, the electrons must maintain their phase as they diffuse over such a path, and therefore the dephasing length L_ϕ must be sufficiently large compared to the elastic mean free path ℓ (only elastic scattering is taken into account in ℓ, while also inelastic processes, such as electron-phonon scattering, contribute to $L_{\rm m}$). The negative magnetoresistance arises because of the suppression of the enhanced back-scattering probability in a magnetic field. The electron waves travelling in opposite directions acquire opposite phase shifts and hence the constructive interference is lost. The conductance of a sample depends on the defect configuration, which is random. The change of magnetic field modifies the phase shift between elastic scattering events so that the scatterer configuration effectively changes, and hence the conductance is altered in a random way. This gives rise to universal conductance fluctuations (UCF). The A-B effect is related to the interference of electron waves travelling along two branches of a ring-like sample.

Electron-electron interactions are especially significant for transport in disordered, low-dimensional conductors [5]. The interactions give rise to a temperature-dependent correction to the conductivity, and also play a key role in the tunneling conductance. In a simplistic interpretation, interactions are enhanced because a pair of electrons remain close to one other for a longer time as they slowly diffuse through a disordered conductor.

If the system is strictly 1D, its ground state is not a Fermi liquid but a so-called Luttinger liquid (LL) [6]. The main characteristic of a Luttinger liquid is that its excitations are plasmons instead of fermion quasi-particles. The density of states near Fermi level is suppressed due to the lack of quasi-particle states. A tunneling experiment between a 3D Fermi liquid and a Luttinger liquid is typically applied to show this suppression. However, this

does not give an unambiguous proof of the existence of the LL state. Another characteristic of the LL is the separation of spin and charge carrying modes, which has not been unambiguously verified for carbon nanotubes.

Length scales and dimensionality

The dimensionality of a sample may vary depending on what type of phenomenon one is looking at. In the case of weak localization, the cut-off is provided by the phase-coherence length L_ϕ. The dimensionality with respect to this effect is determined by a comparison between L_ϕ and the physical dimensions of the sample [7]. In addition, if L_ϕ is longer than the localization length $L_{\rm loc} = ML_{\rm m}$, the strong localization regime is entered and the conductivity is suppressed exponentially as a function of the wire length. The dimensionality of the interaction correction is determined by $L_\epsilon = \sqrt{\hbar D/\epsilon}$, which depends on the range of electron energies available, $\epsilon = \hbar\omega$, $k_{\rm B}T$, or eV, depending on the type of experiment. The dimensionality may be different from that of the weak localization effect. Another scale of importance is the energy relaxation length L_{e-e}, defined as the length over which an electronic excitation relaxes via the inelastic electron-electron collisions, i. e. the electrons thermalize and the Fermi distribution is reached. The electron-phonon scattering length $L_{\rm e-ph}$ determines the resistivity in typical metals, together with the elastic length ℓ, but it is also of importance when dissipation of power is under consideration.

Tunnel junctions

A single-electron transistor (SET) is a device consisting of an island, which is coupled to drain and source electrodes via small tunnel junctions. When the total capacitance C_Σ of the island is small enough so that the charging energy $e^2/2C_\Sigma \gg k_{\rm B}T$ the tunneling at low voltages is not energetically favorable and thus the current is blockaded. A gate electrode is applied to capacitively couple charges even smaller than the electron charge e to the island, and is thus utilized to control the flow of current through the device. The blockade is lifted for island charges $Q = (n+\frac{1}{2})e$, and therefore the current is modulated periodically as a function of gate voltage. Carbon nanotubes can be used to construct single-electron transistors [8–10], where the nanotube forms the central island.

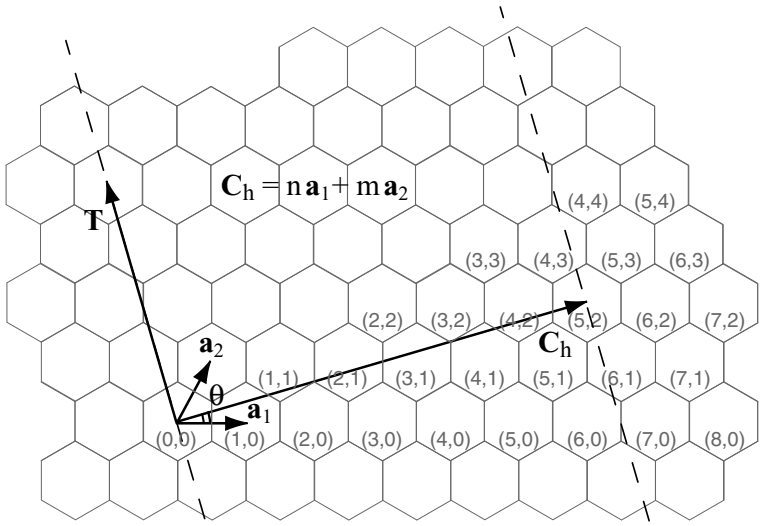

Figure 1.1: Scrolling of a graphene sheet to obtain a carbon nanotube with chiral vector $\mathbf{C}_\mathrm{h} = (5, 2)$. The chiral angle θ is defined as the angle between the lattice vector $\mathbf{a}_1$ and $\mathbf{C}_\mathrm{h}$. For $\theta = 0°$ ($\mathbf{C}_\mathrm{h} = (n, 0)$) and $\theta = 30°$ ($\mathbf{C}_\mathrm{h} = (n, n)$) one obtains especially symmetric structures, called zigzag and armchair nanotubes. The translational vector $\mathbf{T}$ shows the length of one unit cell. The diameter of a (5, 2)-tube is 0.5 nm. A nanotube as small as that can be encountered as the innermost tube in a MWNT[13].

1.2 Carbon nanotubes

1.2.1 Structure

Carbon nanotubes are similar to graphite in the sense that they both consist of carbon sheets with hexagonal lattice, where each carbon atom is covalently bonded to three nearest neighbors. While in graphite these so-called graphene sheets are stacked, carbon nanotubes are formed by rolling the sheet into a seamless cylinder, whose ends are usually closed by a spherical cap. One such tube is called a single-walled nanotube (SWNT), while by arranging several tubes coaxially one obtains a multiwalled nanotube (MWNT). Typically the diameter of a SWNT is 1-2 nm while the MWNTs have diameters of 5-50 nm. Depending on how the axis of the nanotube is directed relative to the lattice vectors of the graphene sheet, one can find nanotubes with different symmetry. Depending on the chirality (see Fig. 1.1) the nanotubes can be either metallic or semiconducting [11]. Tight-binding calculation of the electronic structure can be found e. g. in Ref. [12].

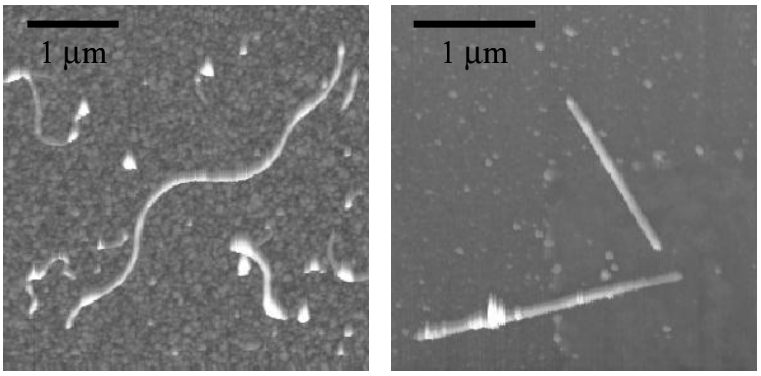

Figure 1.2: Comparison of CVD grown (on the left) and arc-discharge-grown (right) nanotubes.

1.2.2 Synthesis

In this Thesis, I have studied two different brands of carbon nanotubes, arc-discharge grown nanotubes from University of Montpellier and CVD grown nanotubes from Facultes Universitaires Notre-Dame de la Paix, Namur. In the arc-discharge (AD) method [1], large current is applied between electrodes of pure graphite in an inert gas atmosphere. The soot that is produced on the negative electrode contains multiwalled nanotubes that have nearly ideal morphology, but also large quantities of amorphous carbon and other carbon species. In the CVD method, acetylene gas is lead to a flow reactor heated to 700 °C containing the supported transition metal catalyst (Co) [14]. Nanotubes are produced at high yield as a result of catalytic decomposition of the carbon-containing gas. This method results in spaghetti-like tangle of nanotubes in various morphologies, containing also ring-like and helical nanotubes [15, 16]. Intrinsic curvature is a result of defects in the graphitic network. Direct measurement of the Young's modulus of some AD and CVD nanotubes has shown that, indeed, the mechanical properties of CVD tubes are inferior [17]. The measurements on the CVD grown nanotubes performed for this Thesis [P1-P4] are the first fully systematic studies on electrical properties of highly disordered carbon nanotubes.

1.2.3 Electronic transport: A short review

Since the earliest transport experiments in nanotubes [18–21] it has been clear that each nanotube is an individual and hence the outcome of an experiment sensitively depends on details of the particular nanotube sample. In these

experiments, all done on MWNTs, the resistivity[1] was found to vary from kilo-ohms to megaohms per micron, and negative [18] as well as positive [19, 21, 22] magnetoresistance was observed. In MWNTs, there are many degrees of freedom: the diameter and chirality of each shell are different, and amount and type of defects varies over a wide range. The difficulty lies in the separation of essential and accidental properties, and in manufacture of samples with repeatable characteristics. The high resistivity observed in the early studies, e. g. 12–86 kΩ/μm for the regular, 'metallic' samples in Ref. [21], suggests that the nanotubes actually contained a large amount of defects.

Diffusive transport in MWNTs was suggested already in 1996 by Langer *et al.* [18]. The nanotubes were found to behave as 2D diffusive metals, which show both weak localization (WL) magnetoresistance and universal conductance fluctuations at low temperatures, with extremely short phase coherence length L_ϕ of 20 nm at 0.3 K. Later on, a similar value of L_ϕ, 15 nm at 2 K, was found in another weak localization study [23]. Bachtold *et al.* observed Aharonov-Bohm oscillations in samples with a higher L_ϕ of 250 nm [24]. Consistently, the nanotubes were found 1D with respect to WL magnetoresistance in Ref. [25]. However, completely different results were obtained on a nanotube contacted by dipping it into liquid metal (Hg): ballistic transport was observed [26]. Accurate measurements of resistance *vs* dipping depth indicate very low resistivity, $\rho < 100$ Ω/μm [27], and thus the mean free path is so long that it is legitimate to refer to the nanotube as ballistic. Apparently the mean free paths are shorter in lithographically contacted nanotubes, and they typically show diffusive electron transport. In such a sample, the voltage drop over the tube has been directly observed by electrostatic force microscope, and it was found linear, with $\rho \sim 10$ kΩ/μm [28].

For CVD grown tubes, there are less reported experiments available than for arc-discharge grown samples. Dai *et al.* [20] measured very high line resistivity for CVD tubes using a conducting AFM probe, $\rho = 60$–400 kΩ/μm. They also noted that tubes which appear structurally defective exhibit higher resistivity, and an individual bend can increase the resistance significantly. In this Thesis work, electronic transport in CVD grown nanotubes has been characterized in detail [P1-P4].

The transport in single-walled nanotubes depends largely on whether the nanotube is semiconducting or not. Typically the semiconducting tubes be-

[1]Because of the ambiguity associated with the determination of the current-carrying cross-section, either 1D resistivity ρ (units Ω/m) or sheet resistivity $R_\Box$ (units Ω) will be used throughout this Thesis.

have as p-type [29] or ambipolar [30, 31] FETs at room temperature, while the metallic nanotubes don't show much gate dependence [32]. Also scanning tunneling microscopy has been utilized to study the electronic strucutre of SWNTs, and both semiconducting and metallic densities of state were observed [33]. At low temperatures, SWNTs were found to behave as quantum dots [9, 34, 35], where the transport occurs via a finite number of electronic states, extending over the entire sample length, in this case over μm length scales. The observation of a power law tunneling anomaly suggests that the electronic system in SWNTs can be described as a Luttinger liquid [36]. Attaching low-ohmic contacts to a SWNT is considerably more difficult than to a MWNT, and it has only been achieved relatively recently [37, 38]. The realization of a Fabry-Perot interference between electron waves reflected at the contacts indicates that the phase coherence in SWNTs is significantly better that in MWNTs. In general, SWNT is a simpler system and their properties are quite well understood by now. However, open questions still remain such as related to superconductivity in SWNTs, reported by Kociak *et al.* [39].

Semiconducting MWNTs are hardly ever observed [25], even though statistically only every third nanotube should be metallic. The controversy about the amount of metallic vs semiconducting nanotubes was solved when it was understood that the nanotubes are doped by oxygen, shifting the Fermi level by 0.3–0.5 eV [40]. Therefore there are more than four conduction channels in MWNTs, and resistances lower than 6.4 kΩ have indeed been measured [24, 41]. Nanotubes can also be deliberately doped [42].

One way to assess the quality of a nanotube is to measure its current carrying ability. A current density as high as 10^9 A/cm^2 is possible in an individual SWNT [43], and good quality MWNTs are able to stand currents as high as 10 mA under ambient conditions [41]. How is this current distributed among the shells? There is evidence that at low temperature and low bias the current is mainly conducted along the outermost shell [24], but at room temperature several shells are contributing as observed by Collins *et al.* [44]. In their experiment, indicating conduction in several shells, the current saturates, and eventually the nanotubes failed at currents around 200 μA. Later on, the large bias current was observed to depend on the diameter and length of the shell, and $I_{\max}$ = 10-60 μA/shell was found [45]. This is in striking contradiction with the experiments on well-conducting nanotubes contacted by dipping into Hg, where the length dependence was found very weak [46]. No saturation was observed before the tubes failed. The measurements were performed under transmission electron microscope and the failure was observed to occur at defects or at the Hg contact, i. e. where power is dissipated. In an idealistic, defect-free nanotube the coupling be-

tween shells should be negligible [47], and Ref. [46] also suggest conduction at the outermost layer only. Recently, nanotubes positioned on top of the electrodes, not touching the substrate, were studied at high bias voltages, and they did not show a complete saturation of current, but only downturn of conductance, up to 675 μA [48].

The tunneling conductivity between a nanotube and a metallic electrode can be used to probe the density of states, similar to an STM experiment [25]. In many cases, a power law tunneling anomaly is observed around zero bias [49–52]. This suppression is a manifestation of the interactions between the tunneling electron and the electron system in the nanotube. At low enough temperatures, Coulomb blockade develops in a double junction geometry, and SETs have been realized with a MWNT as the central island [10, 53]. When the contacts become more transparent, the complexity of the characteristics increase [54]. In Refs. [55, 56] MWNTs were found to behave as quantum dots, so that they can be clean enough, even when lithographically contacted, to have well defined states that extend over the entire length of the nanotube. As the coupling to the electrodes was quite strong, also the Kondo effect was observable.

2 Experimental techniques

To measure the electrical characteristics of a nanotube, it must be connected to a pair of electrical conduits, connected to the macroscopic measurement electronics. Contacting individual MWNTs was achieved for the first time in 1996 [18–21], and by now the techniques are quite well established. There are two different basic approaches, both of which were utilized in this Thesis work. The first one is to first prepare the electrodes, with a suitable spacing depending on the length of the available nanotubes, and then deposit the nanotubes. One near-by nanotube is moved between the electrodes by utilizing atomic force microscope (AFM) manipulation[10, 57]. The second method utilizes AFM to locate the deposited nanotubes with respect to alignment markers, and the electrodes are subsequently fabricated on top of the nanotubes.

The electrodes are manufactured using standard e-beam lithography. A PMMA resist is spun on a piece of an oxidized silicon wafer. Then the pattern is exposed using a scanning electron microscope (Jeol JSM-6400), and the exposed resist is removed by a suitable solvent. A thin metal film is evaporated using Edwards 306 vacuum coater. The electrode thickness was typically 20-80 nm. Thinner electrodes are needed if one wishes to push a nanotube on top of the electrodes afterwards. After a lift-off in acetone the electrodes are ready.

The nanotubes come in the form of a black powder, which is mixed to a solvent (e. g. dichloroethane) using ultrasonic agitation. A droplet of this dispersion is placed onto the substrate, and after evaporation of the solvent, the nanotubes are left on the chip, randomly placed. It is also possible to use a spinner to apply the dispersion.

The AFM was developed in 1986 [58], and it has become a powerful tool in the research of nano-scale structures (see, e. g. [59]). Unlike scanning tunneling microscope, which was developed earlier, AFM enables also imaging of insulating surfaces. The force between the sample surface and a sharp tip, attached to a small cantilever, causes the cantilever to bend, which can be detected by e. g. optical means. The applied force, which is typically a

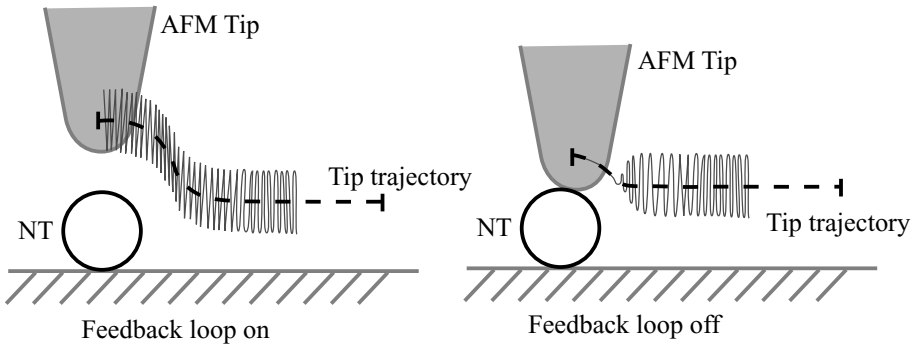

Figure 2.1: The principle of moving nanotubes by AFM (not to scale). On the left, during the usual imaging in the non-contact mode, a feedback loop is utilized to keep the oscillation amplitude (and the tip-surface separation) constant. On the right, the feedback loop is disabled, and the tip comes to contact with the nanotube.

few nN's, is kept constant by regulating the tip-sample distance, and a 3D image of the sample topography is obtained. In the non-contact operating mode, the cantilever is driven to oscillate near its resonant frequency, and the amplitude of the oscillation is monitored. The resonant frequency shifts proportionally to the force gradient, and the observed amplitude changes. By keeping the amplitude constant one can measure a constant force gradient surface. Usually van der Waals forces give the most significant contribution in the non-contact regime, and the measured surface gives the sample topography.

In addition to the usual imaging, AFM can also be utilized in construction of samples as described by Martin *et al.* [57] and Roschier *et al.* [10]. In this approach, small particles or nanotubes are moved in the non-contact mode. The principle is illustrated in Fig. 2.1. The benefit of this method is that it enables to a certain degree monitoring of the nanotube during the movement, and reduces the need to acquire images between manipulation steps. Fig. 2.2 illustrates how the arc-discharge grown tubes behave under mechanical manipulation. Very short nanotubes move as a whole [10], but longer nanotubes bend and show sharp kinks.

The quality of the contacts between the nanotube and the metal electrodes is critical for the outcome of the experiments. In the tube-on-top geometry, contacts are typically very weak. After deposition the resistances range from tens of kΩ's to unmeasurably high. An additional heat treatment (in an evacuated tube oven at $\sim$ 700 °C for a short time, on the order of 30 s [60]) is necessary to reduce the contact resistances. Still, even after this

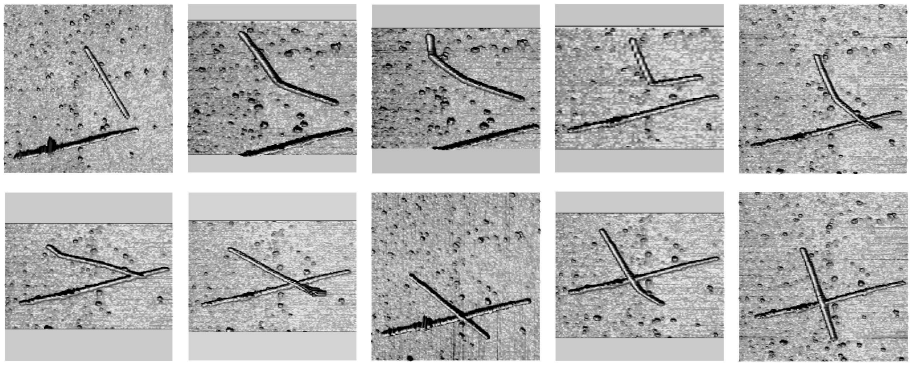

Figure 2.2: Construction of the nanotube cross studied in P7 using AFM manipulation.

treatment tunnel junction typically remains between the nanotube and the metal electrode, and the range of sample resistances remains quite wide. Low contact resistances in the tube-on-top configuration have been reached using a special technique, where the nanotube is 'soldered' to the electrodes by a focused laser beam [22, 39].

On the contrary, depositing electrodes on top of the nanotubes typically results in reasonably good electrical contact even without further treatment. On disordered samples, a heat treatment in air was used prior to evaporation of contacts, which were fabricated using Ti sticking layer, and using this method the outcome was of quite uniform quality, with contact resistances on the order of 1 kΩ. Measurements on samples with such low ohmic contacts is the topic of Ch. 3.

Until now, the fabrication of tunnel junctions on carbon nanotubes has mainly relied on tunnel junctions occurring accidentally. In P5 another approach was attempted. The idea was to use aluminum as the contact material, and see if the formation of oxide would increase the contact resistances over time. Even though aging of contacts was indeed observed, most of the samples manufactured using aluminum contacts were not working in the first place, so no definite conclusions can be drawn about the potential of this method. A summary of the samples studied in this Thesis is given in Table 2.1.

For electrical measurements, the silicon chip with the nanotube is glued to a sample holder, and the measurement leads are connected using a wire bonder. The sample is surrounded by a copper radiation shield. The sample holder is mounted on a dilution refrigerator, which is capable of reaching a base temperature of $\sim$ 100 mK. The measurement lines are filtered by ther-

mocoax cable heat sunk at the mixing chamber. Below 4 K, the temperature is monitored by a Matsushita resistor, calibrated against a Coulomb blockade thermometer [61]. At higher temperatures a calibrated diode [62] is used. Typically both dc and ac resistance are recorded in a two-lead configuration (Fig. 2.3).

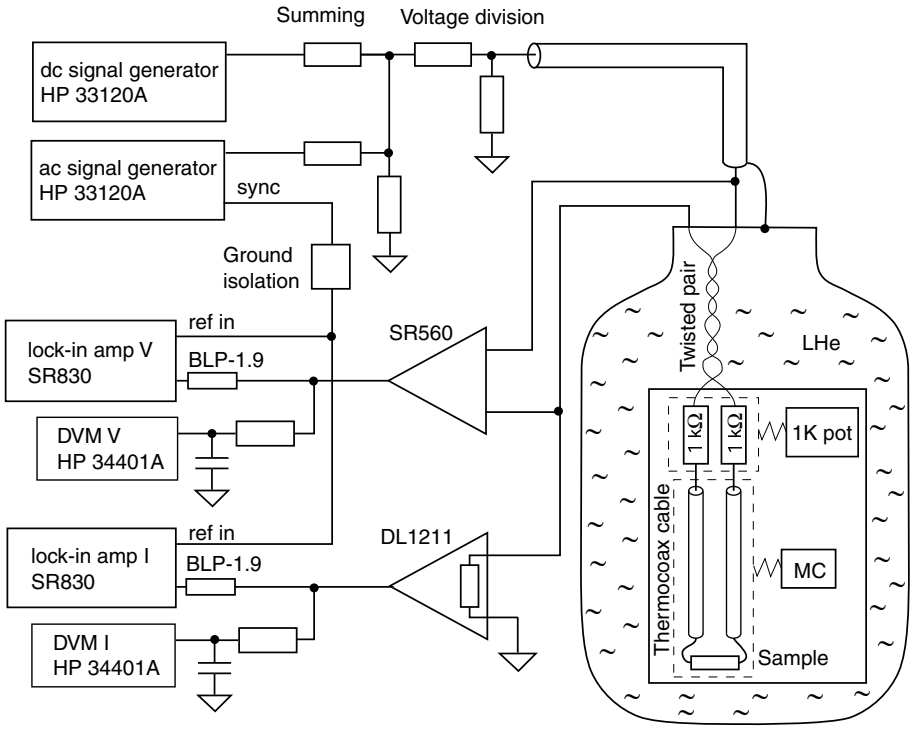

Figure 2.3: The measurement setup. Typically samples were measured in a 2-lead configuration. For the best results the preamplifiers have to be battery-operated. To avoid ground loops, all the measurement electronics is floating, and the setup is grounded via the dewar.

Table 2.1: Summary of the samples. L refers to the length between the contacts, and $R_{295\mathrm{K}}$ is the 2-probe resistance at room temperature. The construction method (nanotube on top (ToT) or electrodes on top (EoT)) and the material of the contacts is given. The synthesis method is either arc-discharge (AD) or chemical vapor deposition (CVD) method. In the last column, the publications containing data on the sample are listed.

Sample	L (μm)	$R_{295\mathrm{K}}$ (kΩ)	contacts	synthesis	References
1	0.50	16.5	EoT, Ti+Au	CVD	[P1, P3]
4	0.38	16	EoT, Ti+Au	CVD	[P1]
6	1.48/1.21[a]	67	EoT, Ti+Au	CVD	[P1]
A	0.77	220[b]	EoT, Al	CVD	[P4]
B	1.9	190	EoT, Al	CVD	[P4]
C	2.8	250	EoT, Al	CVD	[P4]
D	0.78	1600	EoT, Ti+Au	CVD	[P4]
T1	0.5	33	ToT, Au	AD	[P5,P9]
T2	0.3	28	ToT, Au	AD	[P5,P6,P8]
T3	0.6	70[c]	ToT, Au	AD	[P5,P9]
T4	0.7	71	EoT, Cr+Au	AD	[P5,P6,P7]

[a] A ring-shaped nanotube.

[b] Measured at 1.3 K.

[c] Measured at 77 K.

3 Transport in disordered nanotubes

The transport in disordered samples is the subject of publications [P1-P3]. The resistivity of these tubes was estimated from 4-lead measurements to be ρ = 30-100 kΩ/μm[1]. This means that the mean free path ℓ is very short, only a few nanometers. The same measurements suggest that the contact resistance $R_C \leq 5$ kΩ, and hence effects that are intrinsic to the nanotubes are studied.

The electrical conductance was characterized as a function of magnetic field, temperature and bias. The characteristics of all measured samples were similar. The resistance increased moderately towards lower temperatures (Fig. 3.3), magnetoresistance was negative and monotonous (Fig. 3.2), and the differential conductance displayed a dip at zero bias (Fig. 3.1). In general, dependence on all parameters was smooth and featureless. This is in accord with the strong elastic scattering.

An example of a multi-probe measurement is shown in Fig. 3.1. Resistances measured using several different electrode configurations are shown. By such measurements it can be established that the resistances over different portions of the nanotube are completely additive. In a three-probe sample, it is possible to extract the resistance of the middle contact (R_{C2} in Fig. 3.1) by leading a current through the middle probe to one of the ends (e. g. I_2 in Fig. 3.1, $I_1 = 0$) and measuring the voltage between the middle probe and the other end: $R_{C2} = (V_2 - V_1)/I_2$. Correct contact resistance is obtained if there is no significant voltage drop across the width of the middle electrode. Similarly, the resistance of one of the tube segments, e. g. R_{2-3}, can be extracted, eliminating the resistance of the central lead and contact R_{C2} (but R_{C3} cannot be separated). As indicated by dashed line in Fig. 3.1, the sum of these two separate measurements quite accurately reproduces the 2-probe resistance over the same segment. Thus the nanotube behaves quite

[1] A value on the order of 100 kΩ/μm was measured on a reactive-ion etched nanotube. Values below 50 kΩ/μm are more typical.

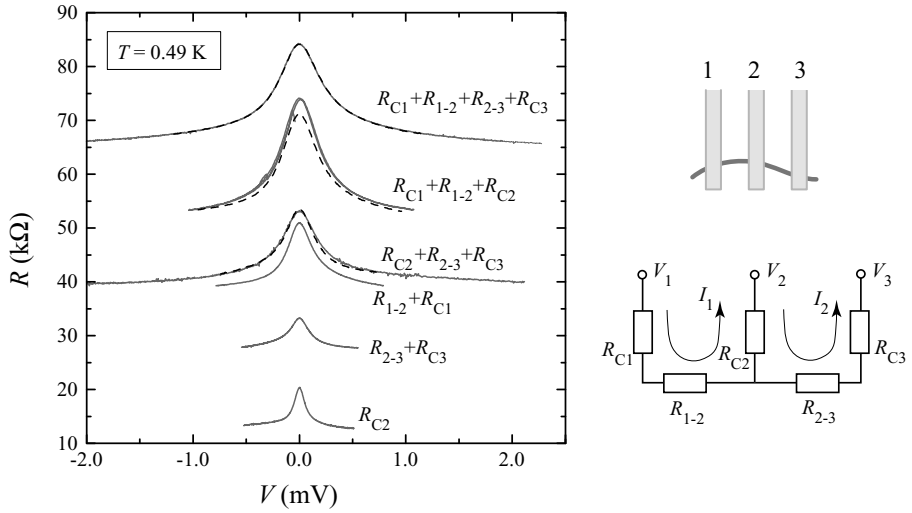

Figure 3.1: The multi-probe measurement does not give much additional information compared with the 2-probe result. The resistances are additive: summation of multi-probe results quite accurately reproduces the two-probe results (sums shown as dashed lines). On the right, schematic of the sample geometry (top) and a circuit model (bottom), defining the various resistances. In a three-probe geometry, only the contact resistance of the central probe can be separated.

a lot like a classical resistor, and the 4-terminal measurements are of limited value (besides extracting a number for R_{C}). The resistivity appears independent of the length, as the size dependent effects are cut-off by the coherence length L_ϕ, which in this case is much shorter than L.

The 4-terminal measurement is not a completely reliable way to determine ρ and R_{C}. The voltage probe does not work as it is intended, if there is current flow in it, and thus the contact resistance cannot be completely eliminated. This occurs for high resistivity samples with wide voltage probes, of width L_{C}, when $\rho L_{\mathrm{C}} \geq R_{\mathrm{C}}$, and finally in the highly disordered limit, when $\rho L_{\mathrm{C}} \gg R_{\mathrm{C}}$, the difference between 2- and 4-terminal measurements disappears. Accidentally, ballistic conductors with ideal contacts also have this feature: 4-terminal measurements do not work there either. The reason is different, however. In a ballistic conductor, one measures in both cases the quantum contact resistance $h/(Me^2)$ of the ideal contacts due to finite number M of channels [2].

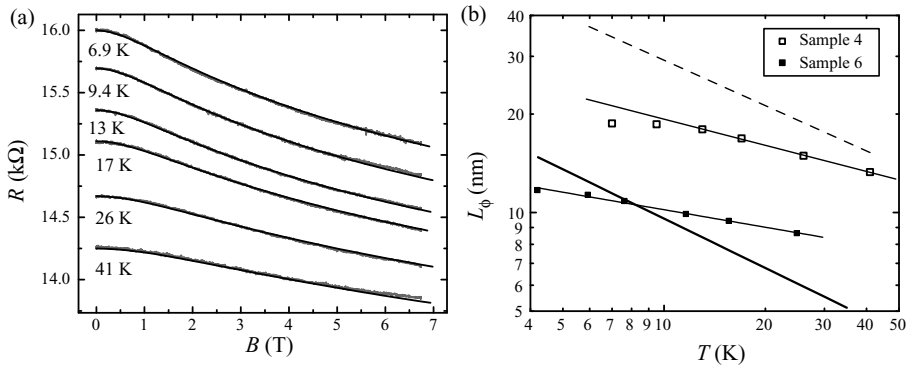

Figure 3.2: (a) Magnetoresistance of a disordered CVD nanotube at a few different temperatures. (b) Phase coherence length extracted from the magnetoresistance shown in (a) (Sample 4) and from another similar set of data (Sample 6). The dashed line is the calculated contribution of 2D e–e scattering for sample 4, and the thick solid line indicates the cross-over from weak to strong localization in the e–e scattering picture.

3.1 Weak localization and magnetoresistance

If weak localization effect is present, the sample is in diffusive regime, and determining L_ϕ gives indirect information about the degree of static disorder in the sample. The magnitude of the correction depends on L_ϕ, and it saturates for very short samples where $L < L_\phi$. In 2D systems, the correction is logarithmic: $\delta\sigma \sim -(e^2/\hbar)\ln(L_\phi/\ell)$ [5].

Applying a magnetic field is useful to study weak localization, as it produces a phase shift to electrons destroying the phase coherence. This gives rise to positive magnetoconductance, which for a 2D conductor in a transverse magnetic field is given by [63]

$$\Delta\sigma(B) = \frac{e^2}{2\pi^2\hbar}\left(\psi\left(\frac{1}{2}+\frac{\hbar}{4eBL_\phi^2}\right)+\ln\left(\frac{4eBL_\phi^2}{\hbar}\right)\right), \qquad (3.1)$$

where ψ is the digamma function. The measured magnetoresistance is shown in Fig. 3.2(a). A good fit to experimental data is obtained using Eq. (3.1), suggesting that 2D description is valid in disordered nanotubes. The dephasing length L_ϕ, shown in Fig. 3.2(b), is obtained as a fitting parameter, and it is consistent with the two-dimensionality assumption: L_ϕ is clearly smaller than the circumference of the nanotube ($\pi\Phi \approx 90$ nm for sample 4). Also fit to 1D theory was tested, but it gives slightly worse fit, and inconsistently with the 1D assumption, L_ϕ is still found smaller than $\pi\Phi$. Universal con-

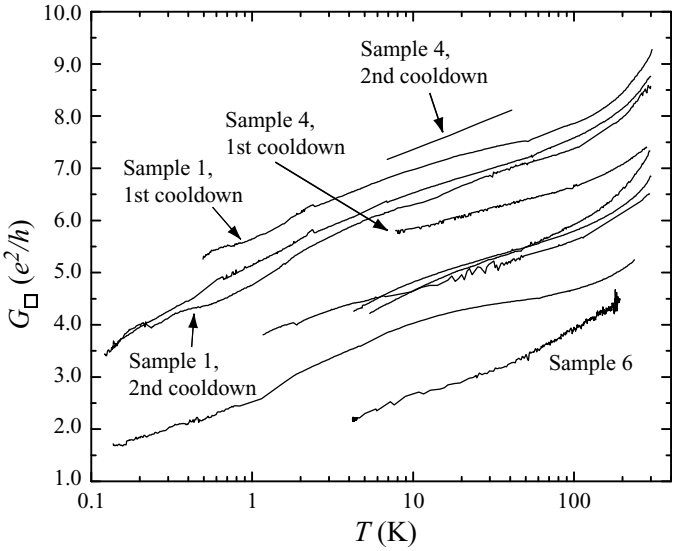

Figure 3.3: Square conductance of several samples as a function of temperature. The logarithmic dependence is visible at lowest temperatures. Two samples are measured twice, in different cooldowns. The resistance shifted slightly over time, probably due to a slight change of contacts during the thermal cycling, but temperature dependence remained similar.

ductance fluctuations were not seen in either of the samples. As L_ϕ is very short, fluctuations are expected to require temperatures lower than 4.2 K, which were not reached in this experiment.

The temperature dependence of L_ϕ is in many cases useful to distinguish between different dephasing mechanisms (phonon, electron-electron or magnetic impurity scattering). In Fig. 3.2(b), the temperature dependence is given by $L_\phi \propto T^{-p/2}$, with $p = 0.36 - 0.53$. This value is smaller than what is expected for phonon scattering or electron-electron scattering [64] (the theoretical prediction for e–e scattering case is shown in Fig. 3.2(b)). The unexpectedly small p leaves a few likely scenarios: there can be large amount of magnetic impurities in the material, or we are observing the break-down of perturbation theory near the strong localization limit.

3.2 Temperature dependence of conductivity

At low temperatures, two quantum corrections are required to the classical conductivity of a disordered conductor, weak localization and interaction corrections [3, 5]. These corrections are especially important for low-dimensional

conductors. The subject of electron-electron interactions is closely related to weak localization, where interactions appear as one contribution to the electron dephasing, in addition to the direct impact they have on the conductivity of the low dimensional system. In 2D conductor, the e–e interaction correction is logarithmic function of temperature, as well as the weak localization correction.

The conductivity of several samples was measured, and in all cases it was found roughly proportional to $\ln T$ (see Fig. 3.3). The localization correction, proportional to the exponent p, is not large enough to account for the entire effect. The remaining part, roughly equal in magnitude, can be assigned to interaction effects. The magnitude of the interaction correction depends on the Fermi liquid interaction parameter F_0^σ, characterizing the screened Coulomb interaction [65], the value of which is not known for nanotubes. Since the pre-factor to the logarithm appears to be similar in all samples, according to the data in Fig. 3.3, it looks like p and F_0^σ don't vary much from sample to sample, in which case the square conductance should show an universal slope.

Even though the experimental findings are in accord with the quantum corrections due to weak localization and electron-electron interactions, there are some complications. The square conductance for some of the samples in Fig. 3.3 is quite low, reaching $2e^2/h$, and therefore they are close to the strong localization limit, where the perturbation theory results [5, 64] no longer apply.

Also it is questionable whether it is reasonable to think about a diffusive conductor with $\ell < 1$ nm: is it more likely that the resistance is located at a few places where the tube is defective and conduction between these scatterers is much better? According to this line of thought, the nanotube could be modelled as an array of tunnel junctions in the strong tunneling regime, a model for which theoretical results have been calculated [66]. Even though G vs T can be fitted, the shortcoming of this model is that it does not account for the magnetic field dependence.

3.3 Heating effects

When performing electrical transport experiments at low temperatures one always has to bear in mind that the electrical current gives rise to power dissipation, with $P = RI^2$. Unless this extra heat is effectively transported to the surroundings, the temperature of the system may rise considerably, which has been directly observed in carbon nanotubes by scanning thermal microscopy [67]. In publication [P3], the role of heating in the disordered

nanotubes is considered by calculating the differential conductance *vs* voltage. Experimentally, the conductance shows a dip around zero-bias (or peak in resistance as in Fig. 3.1), reminiscent of the well-known tunneling anomaly, but as it appears even in the absence of tunnel junctions, it must be accounted for as a manifestation of electron heating. Another possible origin of the dip is an electron-electron interaction related correction to conductivity, but heating seems more likely.

A hot electron in the nanotube can lose its energy via scattering with phonons, and lattice must dissipate this energy to the substrate or electrodes. In a steady state, two separate regimes can be distinguished depending on the relative magnitude of the coupling between electrons/phonons and phonons/substrate [68]. If the electron/phonon coupling is strong, which is typically the case at room temperature, lattice temperature T_0 and electron temperature T_e are practically equal and the system heats as a whole. On the contrary, if electron-phonon scattering is weak, the electron temperature T_e may rise considerably above T_0. At low temperatures electron-phonon scattering quickly becomes weak and electron heating becomes more significant.

In addition to electron-phonon scattering, the electron system can also cool down via electronic thermal conduction. The nanotube is connected to electrodes which can be considered as thermal reservoirs where the heating is negligible, since they have much larger volume and smaller resistance than the nanotube. Hence the ends of the nanotube remain at lattice temperature T_0 and a temperature profile is created over the nanotube (Fig. 3.4). The one-dimensional thermal diffusion equation can be written as

$$\frac{\pi^2 k_{\mathrm{B}}^2}{6e^2}\frac{d}{dx}\left(\sigma(T_{\mathrm{e}}(x))\frac{dT_{\mathrm{e}}^2}{dx}\right) = -\rho(T_{\mathrm{e}}(x))I^2 + A\Sigma(T_{\mathrm{e}}(x)^5 - T_0^5), \qquad (3.2)$$

where the first term on the right gives the power generated in the nanotube ($\rho(T_e) = 1/\sigma(T_e)$ is the temperature-dependent resistivity of the nanotube), and the second one gives the energy flow from electron system to phonons [68], and Σ is the electron-phonon coupling parameter.

Several assumptions are done in this model. 1) It is necessary that a position dependent electron temperature exists. This is the case if energy relaxation length L_{e-e}, over which the thermal distribution is established [69], is much shorter than the sample length L. 2) The electron thermal conductivity is given by the Wiedemann-Franz (WF) law. 3) The thermal resistance, which the electrons experience at the contacts, is negligible (generalization is possible and yields only a small change to final results as long as the thermal resistances remain 'small'). 4) The form of the electron phonon-coupling in

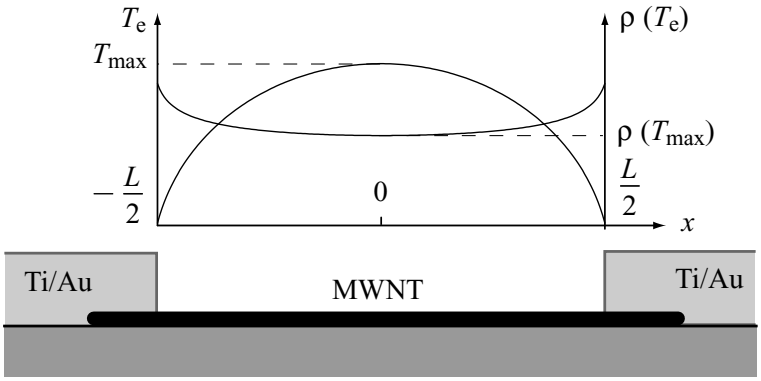

Figure 3.4: The temperature profile along the nanotube when current is passed through it. For modelling purposes it is assumed that the temperature dependent resistivity also changes along the nanotube.

Eq. (3.2) is deduced for clean metals. For disordered and/or low-dimensional conductors, the exponent may differ from 5.

Equation (3.2) enables numerical calculation of the temperature distribution in a nanotube. To make connection with the experiment, the differential resistance *vs* bias voltage must be estimated. By assuming that the resistivity (units Ω/m) is a function of the local temperature (see Fig. 3.4), and integrating over the nanotube length, the total resistance R_{NT} and hence the voltage $V = R_{NT}I$ *vs* the heating current can be obtained. The differential conductance dI/dV is calculated by numerical differentiation. The input to such a calculation is the experimentally determined temperature dependence of conductivity, which in this case is logarithmic (Fig. 3.5(a)). Comparison with experimental G–V-curves is shown in Fig. 3.5(b). At low heating currents the electronic thermal conduction is more efficient and $T_e \propto V$ (implying that $G(V) \propto G(T)$). However, at higher bias the heating slows down as the phonon scattering mechanism becomes more significant and $T_e \propto V^{2/5}$.

For the sample in Fig. 3.5, the fit gives $\Sigma = 0.23$ nWμm^{-3}K^{-5}, which is slightly less than a typical value for metals, 1 nWμm^{-3}K^{-5}. The value depends on how one chooses to calculate for the cross-sectional area A of the nanotube. Here a circular cross-section was used. Since the conduction is supposed to take place mainly in the outermost layer of the nanotube, the effective volume where energy exchange can occur is actually smaller than AL. Thus Σ is somewhat underestimated. The coupling per unit length for this sample is $A\Sigma = 0.15$ pWμm^{-1}K^{-5}.

In the simulated temperature of Fig. 3.5(a) there is a cross-over from $T_e \propto V$ to the phonon limited case $T_e \propto V^{2/5}$, and corresponding cross-over

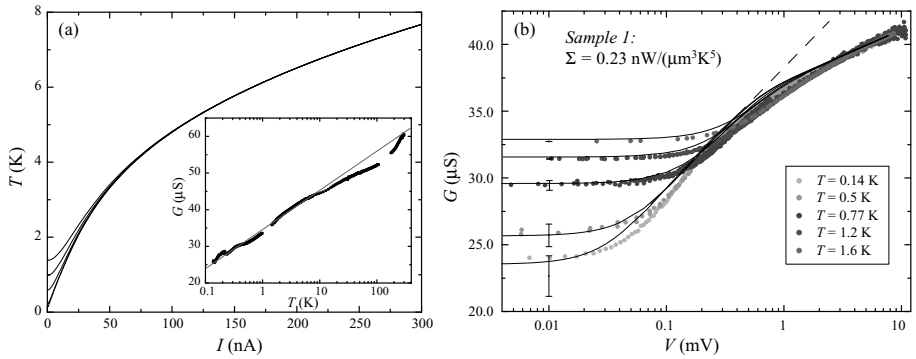

Figure 3.5: (a) Maximum electron temperature in a resistive carbon nanotube as calculated from the heating model. The lattice temperature T_0 is varied between 0.13 and 1.4 K. Inset: Zero-bias conductance *vs* temperature of the nanotube. Straight line is a logarithmic least squares fit, which enters into the simulation. (b) Conductance *vs* bias voltage at a few different temperatures. The solid lines are the simulated curves, calculated from the heating model using the fit shown in (a) for the temperature dependence of conductance. The behavior in the absence of electron-phonon scattering is sketched as a dashed line. The bars indicate the range of conductance modulation by a side gate at zero bias.

is visible in the measured resistance as well (the behavior when electron-phonon scattering is neglected is sketched as a dashed line in Fig. 3.5(b)). One has $L_{e-ph} \simeq L$ at the cross-over. One can also estimate L_{e-ph} at this temperature: according to the theory [68] $L_{e-ph} = 1.313 k_B/(e\sqrt{\rho(T_e)T_e^3 A\Sigma}) \approx$ 240 nm ($T_e \sim 3$ K), which indeed is quite close to the sample length (L = 0.5 μm). Since the scattering length appears to be this long, it is quite understandable that the electron-phonon scattering only becomes important at higher temperatures from the dephasing point of view.

What should the exponent n of phonon coupling term be? Experimental data suggests that $n = 5$ works quite well, but also $n = 4$ is possible. Exponent $n = 5$ is based on the three dimensional independent electron theory. It may not be entirely valid for carbon nanotubes, since the phonon coupling is probably somewhat different. There is, however, no theoretical calculations available for nanotubes in the disordered limit.

While WF law has been shown to remain valid for weak localization correction [70], theoretical calculations predict that it does not hold for disordered conductors, where electron-electron interaction correction is significant, and an additional interaction correction to the thermal conductivity κ is required [71]. Applying the correction for interaction in 2D, given in

Ref. [71], with parameters applicable to our samples, it turns out that the error in omitting this correction is less that 5% at 1 K, so using the WF law is a good enough approximation. The relative error increases towards lower temperatures, with weak logarithmic temperature dependence.

Self-heating in a suspended wire has been applied as a method to extract the thermal conductivity of a conductor [72]. Basically the method is a measurement of heating induced differential conductance change, similar to what is done here on nanotubes. Here, however, electronic thermal conductivity is assessed, because the temperature of the phonons is lower. For the self-heating method to work, it is necessary that there is no other non-linearity in the IV-characteristics, such as Coulomb blockade. If this is not the case, then this method fails, because it cannot specify the origin of the non-linearity. Similarly, the non-linearity of the IV-characteristics, such as that in Fig. 3.5(b), can be taken as a demonstration that thermal conductivity of our samples is roughly given by the Wiedemann-Franz law, but it is not accurate enough to measure small deviations thereof.

At high currents, the temperature gradients produced by the numerical model become very steep and, as such, cannot reflect any true temperature change in the carbon nanotube. In such a case it is sufficient to neglect the gradient altogether and assume a constant temperature $T_e = \sqrt[5]{T_0^5 + P(T_e)/\Sigma AL}$ over the nanotube.

4 Zero-bias tunneling anomalies

The appearance of a dip in the tunneling conductance around zero bias is a manifestation of the e–e interactions. This phenomenon has been known in large metal-insulator-metal junctions already for a long time, and it is discussed at length in Ref. [5]. Due to the interactions, the electron system of a diffusive electrode must relax after a tunneling event in order to accommodate the tunneling charge. Another related anomaly appears in ultra-small tunnel junctions with small capacitance C_{T}: due to charging of the junction capacitance the tunneling of electrons with energy below the Coulomb energy $E_{\mathrm{C}} = e^2/2C_{\mathrm{T}}$ can be completely blocked until the charge has relaxed via an external circuit. The tunneling rate is related to the dissipation in the external electromagnetic environment, whose effect is to damp fluctuations of the tunnel junction charge. The theory is discussed in Ref. [73], and it is sometimes referred to as environmental quantum fluctuation theory (EQFT). In both disorder enhanced tunneling anomalies and EQFT, tunneling between two usual Fermi liquids is under consideration. In a strictly 1D conductor where the ground state is a Luttinger liquid [6] instead of Fermi liquid, a third type of anomaly is predicted to occur: the tunneling is suppressed due to the lack of low energy excitations (quasi-particles) in a Luttinger liquid. In this chapter, the tunneling anomaly between a MWNT and a metal electrode is discussed, and a short note about the relevance of the Luttinger liquid model in MWNTs is given.

The suppression of the tunneling between disordered electrodes becomes stronger as disorder increases. This can be understood because scattering events slow down the spreading of charge after tunneling. The effect depends on the geometry of the conductors in which charge relaxation occurs. The effective dimensionality of the conductors is determined by the Thouless energy for the field diffusion: $E^*_{\mathrm{Th}} = \hbar D^*/x^2$, where D^* is the field diffusion coefficient, and x is a characteristic dimension of the wire, i. e. either thickness, width or length [74, 75]. Using plasmons in the over-damped

case, it can be estimated that $D^* \approx 1/rc_\mathrm{T}$, where r is the resistance of the wire and c_T is the capacitance of the junction, both per unit length. The dimension decreases by one, whenever the energy scale of the tunneling electron (either eV or $k_\mathrm{B}T$, whichever is larger) becomes smaller than the Thouless energy E^*_Th corresponding to one of the sample dimensions. In disordered nanotubes, the relevant cases are one-dimensional junctions, i. e. when $\hbar D^*/L_\mathrm{C}^2 < \epsilon < \hbar D^*/w_\mathrm{eff}^2$, and zero-dimensional junctions, $\epsilon < \hbar D^*/L_\mathrm{C}^2$. Here L_C is the length, and w_eff is an effective width of the junctions.

At low enough energies one arrives at the 0D limit, $L_\mathrm{C} < \sqrt{\hbar D^*/\epsilon} = L^*_\mathrm{Th}$, where the charge spreading over the junction can be considered instantaneous, and the behavior is described by the EQFT. The suppression of tunneling is strong if the electromagnetic environment of the junction has a high resistance $R_\mathrm{env} \gtrsim R_\mathrm{K} = h/e^2$. On the low-$R_\mathrm{env}$ limit the IV-characteristics approach linear behavior. The isolating resistance must be located close to the junction. Experimentally, it is possible to reach complete Coulomb blockade using an ohmic resistor [76]. More typically, isolation is provided by another tunnel junction, and one deals with a single-electron transistor (see Ch. 5).

4.1 1D junctions

The finite length tunnel junction between a bulky metallic electrode and a resistive carbon nanotube can be modelled by the circuit of Fig. 4.1(b). This model considers the nanotube as a finite length RC-transmission line with a distributed resistance r and capacitance c, and a higher capacitance c_T in the section which is in contact with the electrodes. The model is rather complicated, and it contains more parameters than can be unambiguously extracted from an experiment. For a more stringent comparison between the theory and the experiment, the number of variables needs to be reduced. The model approaches two convenient limiting cases at very high and very low energies: when $\epsilon \gg \hbar D^*/L_\mathrm{C}^2$, the 1D tunnel junction is effectively infinite (Fig. 4.1(c)), and when $\epsilon < \hbar D^*/L_\mathrm{C}^2$, the junction is zero-dimensional and the electromagnetic environment determines the tunneling conductivity (Fig. 4.1(d)). These two cases have been compared with experiments in publication [P4].

The samples in [P4] were manufactured using CVD grown tubes. In order to study 1D junctions over as wide energy range as possible, the contacts were made relatively wide (0.6-1.1 μm). Therefore also the nanotubes selected for this experiment were among the longest found in the source material (2.5-9 μm). The inherent difficulty here is that the resistance of the nanotube

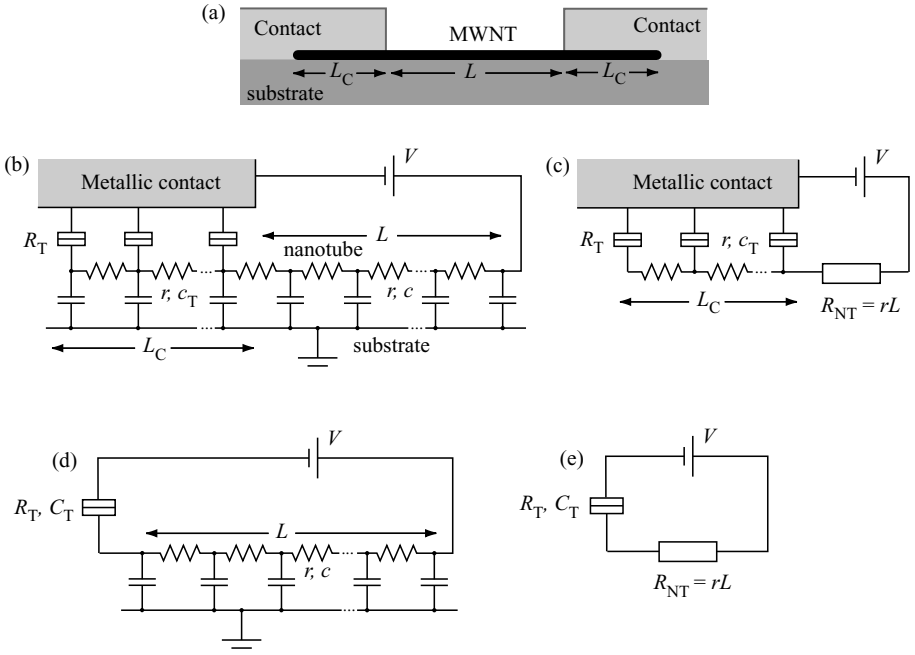

Figure 4.1: (a) A schematic geometry of a MWNT contacted by two metallic electrodes. (b) Corresponding circuit model of the tunnel junction between a resistive carbon nanotube and a bulky metallic electrode. For simplicity, one of the junctions is neglected, which is legitimate assuming that $R_{T1} \gg R_{T2}$. (c) At high energies, the junction is effectively infinitely long ($L^*_{\rm Th} \ll L_{\rm C}$) and the environment does not affect the tunneling. The environment can be replaced by a lumped resistor $R_{\rm NT}$, or, if $R_{\rm NT} \ll R_{\rm T}$, neglected entirely. (d) At low energies the junction can be considered small ($L^*_{\rm Th} \gg L_{\rm C}$), and replaced by a lumped element tunnel junction. The environment determines the suppression of tunneling conductivity. (e) At even lower energies, the finite length transmission line can be replaced by a lumped element resistor.

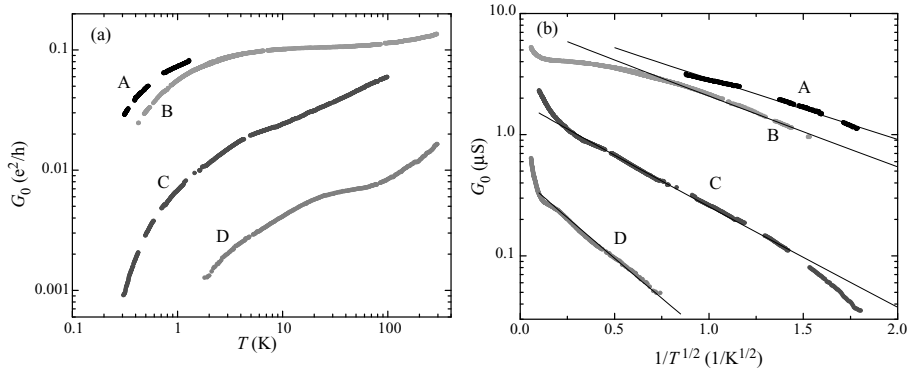

Figure 4.2: Tunneling conductance vs temperature. For details of samples, see Table 2.1. For the fits, see text.

$R_{\rm NT}$ is quite large, and, as discussed in Ch. 3, it also depends on V and T. Therefore the tunneling resistances have to be quite high, so that the tunneling effects govern the conductivity. In [P4] this was achieved by using aluminum as the electrode material. The tendency of Al contacts to oxidize in air was utilized if too low $R_{\rm T}$ was obtained initially.

The measured tunneling conductance of several samples is shown in Fig. 4.2(a). In comparison to the behavior in Fig. 3.3 in Sec. 3.2, the temperature dependence is now much stronger (also the two-probe resistance of these samples is larger than those considered in Sec. 3.2, see also Table 2.1), which suggests that the tunnel junctions dominate the results, and it is a reasonable first-order approximation to neglect the logarithmic corrections to $R_{\rm NT}$.

The plot in Fig. 4.2(b) shows that the tunneling conductivity is roughly given by $G \propto \exp(-\sqrt{T_0/T})$. Similar results have been reported for boron-doped MWNTs [77]. The results are compared against the theoretical calculations for infinite 1D junctions [78, 79]. While in a metallic junction the perturbative techniques of Ref. [5] have proven sufficient, the anomaly in disordered nanotubes is strong enough to call for a non-perturbative treatment. The solid lines in Fig. 4.2(b) are calculated according to Refs. [78, 79], and over the energy range of 0.5-100 K the agreement between theory and experiment is good in all samples except for sample B, for which good fit cannot be reached over a wide temperature range.

Both the voltage and the temperature dependence of the tunneling conductivity can be fitted by the non-perturbative theory, within the experimental accuracy. However the inaccuracy in the case of voltage dependence is considerable, because of the irregular fluctuations in the conductance. In Fig. 4.3, the GV-characteristics of two of our samples are shown, clearly illustrat-

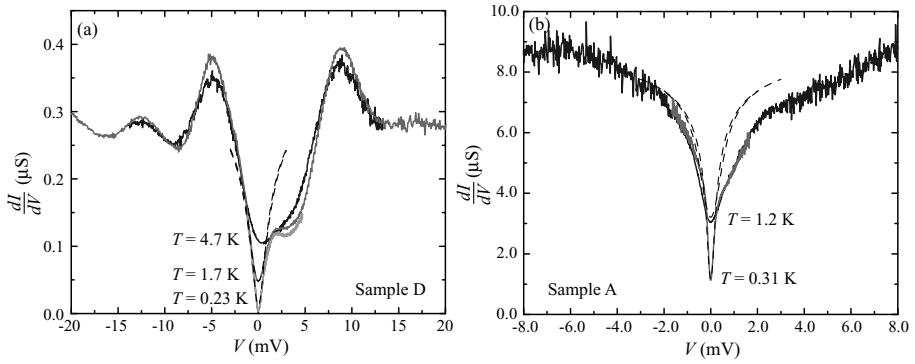

Figure 4.3: GV-characteristics of two of the samples of publication [P4]. The irregular features are more clearly visible in the sample on the left, which is typical for samples with high resistance. The dashed lines have been calculated using the 1D tunneling theory, with the same parameters as in Fig. 4.2(b).

ing that accurate fitting of the data using a symmetric, monotonic function is not possible. In theoretical work, such as Refs. [78, 79], it is customary to assume the tunneling matrix element to be an energy independent constant which is absorbed into the tunneling resistance R_{T}. The behavior in Fig. 4.3 suggests that this assumption is not valid for disordered MWNTs. One possibility is that the transmissions of the contacts experience resonant behavior due to localized states in the junction area. In addition, the detailed structure may vary when the contacts change, e. g., due to thermal cycling.

4.2 0D junctions

In the case of a small tunnel junction, $L^*_{\mathrm{Th}} \gg L_{\mathrm{C}}$, the functional form of the anomaly is determined by the electromagnetic environment of the junction, which is formed by the nanotube. The suitable circuit model depends on the nanotube material. In [P4], the EQFT was applied to a disordered nanotube using an RC-transmission line environment (Fig. 4.1(d)). In [P5], arc-discharge tubes were analyzed using an LC-transmission line model (obtained by replacing the distributed resistance r in Fig. 4.1(d) by distributed inductance l). There is an interesting connection between the latter description and the Luttinger liquid model, since the excitations in a Luttinger liquid are plasmons, which are similar to the propagating electrodynamic modes in usual LC-transmission lines. This will be discussed in Sec. 4.3.

According to the environmental quantum fluctuation theory, conductance

of a tunnel junction is given by [73, 80]

$$\frac{dI(V)}{dV} = \frac{1}{R_{\mathrm{T}}}\left[1 + 2\int_0^\infty \frac{dt}{\hbar\beta}\frac{\pi t}{\hbar\beta}\mathrm{Im}\left\{e^{J(t)}\right\}\frac{\cos(eVt/\hbar)}{\sinh^2(\pi t/(\hbar\beta))}\right], \tag{4.1}$$

where $\beta = 1/k_{\mathrm{B}}T$ and $J(t)$ is the phase correlation function, related to the circuit impedance via the fluctuation-dissipation theorem [73]:

$$J(t) = 2\int_0^\infty \frac{d\omega}{\omega}\frac{\mathrm{Re}\left\{Z_{\mathrm{t}}(\omega)\right\}}{R_{\mathrm{K}}}\left\{\frac{\cos(\omega t) - 1}{\tanh(\beta\hbar\omega/2)} - i\sin(\omega t)\right\}. \tag{4.2}$$

The total impedance seen by the junction, $Z_{\mathrm{t}}(\omega)$, consists of the external impedance in parallel with the tunnel junction capacitance C_{T}.

Tunneling into high resistivity nanotubes

In [P4], the 0D model was applied to one sample, which did not follow the 1D theory very well (sample B in Fig. 4.2(b)). It is not completely clear how this sample is different from all the others, but most likely one of the contacts is actually shorter than it appears to be in the AFM images, giving rise to the 0D behavior. The nanotube impedance was modelled by an RC-transmission line, which is a good model for a disordered carbon nanotube. One junction model was assumed, which is valid if the contact resistances are highly asymmetric. As shown in Fig. 4.4(b), the 0D model gives a good fit with reasonable set of parameters. Also a simpler circuit model, an ohmic resistor, could have been used, as shown in Fig. 4.4(a). This model is especially straightforward to apply as an analytic expression for the integral of Eq. (4.2) exists [80]. The fit is only slightly inferior, and it has one fitting parameter less. The difference is quite insignificant and similar parameters are obtained in both cases.

The temperature dependence of conductance for sample B is roughly given by $G \propto \exp(-T_0/T)$ at high T, which is also characteristic for a SET. Actually, when $R_{\mathrm{env}} \geq R_{\mathrm{K}}$, the conductance of a single tunnel junction in series with a resistor behaves just like a SET as a function of temperature, in the high temperatures range, where there is no gate modulation [80]. However, a simple two-junction SET model is not applicable. A SET constructed using a disordered nanotube, assuming that the junctions are located between the electrodes and the nanotube, differs from the regular case. First of all, as seen in the model calculation of Fig. 4.4, the nanotube resistance itself is high enough to give rise to environmental Coulomb blockade. This should appear as an additional suppression of conductance, which cannot be lifted by the gate voltage. Also, the characteristics become rounded due to the

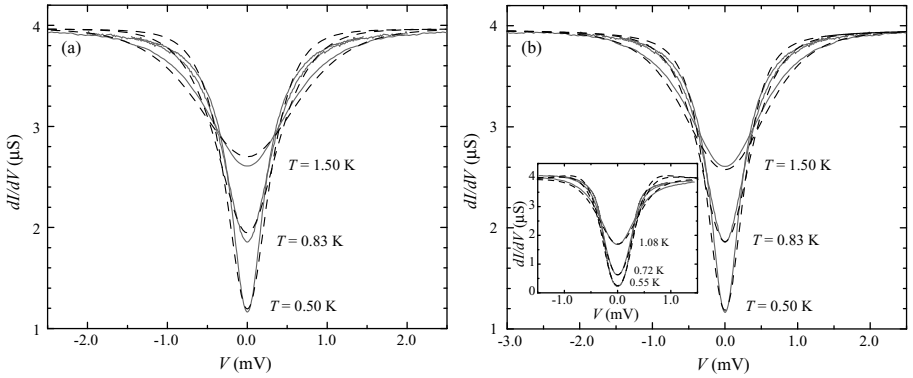

Figure 4.4: 0D tunneling modelled by (a) a lumped resistor model ($R_{NT} = 117$ kΩ, $R_T = 135$ kΩ, and $C_T = 300$ aF, the model is sketched in Fig. 4.1(e)), and (b) RC-transmission line model ($R_{NT} = 90$ kΩ, $R_T = 162$ kΩ, $C_T = 260$ aF, $r = 45$ kΩ/μm, and $c = 240$ aF/μm, see Fig. 4.1(d)). The inset shows the fit in the case of superconducting electrodes, using the same parameters as the main frame. The experimental data for sample B is shown as solid lines, while the theoretical fits are shown as dashed lines.

resistive environment, and the amplitude of the gate oscillations is reduced [73]. Returning to the RC-line description, the electromagnetic signal propagates in the nanotube with velocity $v_{\rm pl} \approx \sqrt{\epsilon/(\hbar r c)}$, and the 'event horizon' of a junction is located a distance $L_{\rm h} = \hbar v_{\rm pl}/\epsilon$ away, where ϵ is the electron energy scale. For a typical sample, the resistivity of the nanotube completely isolates the junctions from one another already at mV energy scale, and they can be treated individually. Accordingly, it is not surprising that no periodic gate modulation was observed in sample B, when voltage was applied to the silicon substrate, functioning as a backgate.

When the resistance of the environment is very large, comparable to the tunnel junction resistance, some part of the charge relaxation occurs through the junction itself. The total impedance $Z_{\rm t}(\omega)$ needs to be corrected by including the resistance of the junction in parallel with the environment [81]. Hence the $R_{\rm env}$ does not necessarily equal the resistance of the nanotube. In the fit depicted in Fig. 4.4(a), $R_{\rm env} \approx R_{\rm NT} \| R_{\rm T}$. Actually, the voltage dependent tunneling resistance $R_{\rm T}(V)$ should be used in parallel with $R_{\rm NT}$, in which case the total conductivity needs to be solved self-consistently [82]. However, as the anomaly is not very sensitive to changes in $R_{\rm env}$ as long as $R_{\rm env} \gtrsim R_{\rm K}$, constant $R_{\rm T}$ is a reasonable first approximation.

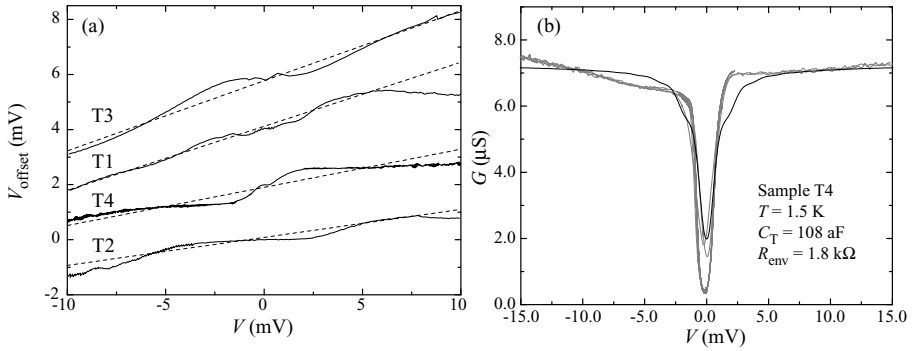

Figure 4.5: (a) Offset voltage $V_{\rm offset} = V - I/(dI/dV)$. The straight lines indicate power law behavior $I \propto V^{\alpha+1}$. (b) GV-characteristics of sample T4 (gray line). The various traces result from random gating by the background charge fluctuations. The theoretical line is calculated for a SET with the parameters shown.

Tunneling into low resistivity nanotubes

Tunneling into a good quality AD nanotubes was studied in [P5]. The tunneling anomaly differs from the above case because the resistivity of the nanotubes is low, and at high frequencies r is not as important as the inductance: $r \leq \omega l$. Due to the low density of charge carriers in a nanotube, the kinetic inductance $l_{\rm kin}$ of nanotubes is much larger than the magnetic inductance. For ballistic SWNTs 16 nH/μm has been calculated [83], but in MWNTs the value is lower due to larger amount of channels and possibly disorder. The impedance of a good quality nanotube, $Z = \sqrt{l_{\rm kin}/c} \sim 5$ kΩ, is low in comparison to typical tunnel junction resistances. Therefore one must consider a model environment consisting of the LC-transmission line in series with the other tunnel junction. Three regimes in conductance can be separated as the bias voltage is varied: (1) At lowest voltages, the junctions 'see' each other and the system becomes a SET, (2) at medium energy range, the conductance of each junction is a power law $G \propto V^{\alpha}$, and (3) at highest energies the conductance approaches Ohm's law asymptotically.

The analysis in [P5] considers the high voltage cases, (2) and (3), where the 'local rule' applies [73, 84], and the junctions can be considered independent. For two junctions in series, one obtains the high-voltage asymptotic behavior

$$I = \frac{1}{2R_T}\left[V - \frac{e}{C_{\rm T}} + \frac{4R_{\rm K}}{Z}\left(\frac{e}{2\pi C_{\rm T}}\right)^2 \frac{1}{V}\right]. \qquad (4.3)$$

The high frequency impedance was found to be $Z = 1.3$-7.7 kΩ. At medium

voltages, when $V \ll \hbar/(eRC_{\rm T})$ and $T = 0$ K, the IV-characteristics are given by a power law $I \propto V^{1+\alpha}$ (see Fig. 4.5(a)), where $\alpha = 2Z/R_{\rm K}$. Fitting of this power law yields an independent estimate for Z, which is found to be consistent with the value deduced from the asymptotic fit. Using a value $c = 70$ aF/μm, $l_{\rm kin}$ was estimated as 0.1-4.2 nH/μm. At even lower voltages, below the plasmon frequency $\omega_{\rm pl} = v_{\rm pl}/L = 1/(\sqrt{cl_{\rm kin}}L)$, the assumption of independent junctions breaks down and SET behavior is expected.

In good-quality nanotubes of finite length, one expects to see steps in the GV-characteristics with spacing $\Delta V = \pi\hbar/(e\sqrt{cl_{\rm kin}}L)$. In most cases these resonances are not seen, possible reasons for that being the small resistivity that remains in the nanotube-transmission line, smearing due to the wide contacts, or leakage of the plasmon modes to the electrodes due to too low $R_{\rm T}$.

At the lowest temperatures the sample is expected to behave as a SET. A comparison between sample T4 (the one with the highest resistance) and the standard SET theory is shown in Fig. 4.5(b). The fit for this sample is tolerable, but for the other samples this approach faces serious difficulties. The Coulomb blockade remains weak as indicated by roughly linear behavior in Fig. 4.5(a), and the junctions stay independent.

4.3 Is Luttinger liquid important for MWNTs?

The ground state of a 1D conductor with arbitrarily weak interactions is a Luttinger liquid (LL). Single-walled nanotubes can be considered as quite good realizations of the Luttinger liquid. The tunneling conductance of SWNTs is suppressed at low energies as a power law: $G \propto V^{\alpha_{\rm LL}}$ or $G \propto T^{\alpha_{\rm LL}}$ [36]. While in metallic SWNTs there are four conduction modes (two spins, two bands crossing at Fermi level), in MWNTs, the number of channels can be tens. Due to their larger diameter, the energy separation between the transverse modes is not very large, and the tubes are typically clearly doped [40], increasing the number of modes. When there is a large amount of channels, the LL exponent $\alpha_{\rm LL}$ decreases as $\propto 1/\sqrt{N}$ [83, 85] and hence the behavior approaches that of a Fermi liquid (in Ref. [85] N is number of shells but it could be number of modes as well). Hence, the exponents should be clearly smaller for MWNTs, on the order of 0.1, which is not in line with experimental observations, which suggest similar exponents for SWNTs ($\alpha_{\rm bulk} \approx 0.3 - 0.4$ [36]) and MWNTs ($\alpha_{\rm bulk} \approx 0.3$ [49]).

The most important factor working against the LL model in MWNTs is scattering. In the theory (see, e. g. [86]), any defects in the LL lead to a power law suppression of conduction. As the theory is strictly one-dimensional,

there is no way the electron can work its way around the defect. At low enough temperatures disorder is predicted to lead to the complete suppression of conductance. The characteristic power law is valid at high energy range $\epsilon \gg \hbar v_{\mathrm{F}}/(\sqrt{N}\ell)$ [79], which for very good quality SWNTs ($\ell \geq 1$ μm) means $T \gg 1$ K, but for disordered MWNTs $T \gg 300$ K, and clearly the LL model is not relevant. The conductivity in the disordered tubes should be completely suppressed, which is not in line with experimental observations. It is possible that, as N is large, there is considerable amount of scattering between the transverse channels in disordered samples. Hence, these samples are not truly 1-dimensional and LL model is not valid at any temperature. In a recent photoemission spectroscopy study, evidence was found that the low energy excitations in MWNTs behave as usual Fermi liquid quasi-particles [87].

The EQFT does produce exactly the same behavior as the LL theory in the large N limit, when both the geometrical and the quantum capacitance of the nanotube are included in the transmission line description [88]. The LL theory can be formulated in electrical engineering terms using transmission line analogy for the plasmon excitations[83]. In addition to the charged mode, there are also neutral modes which do not carry charge but can carry spin. Comparing the supposed LL state in MWNTs and SWNTs by their respective transmission line parameters, l_{kin} is reduced in MWNTs due to the larger number of modes (as found in [P5]), and, importantly, c should be larger due to the size of the conductor and the screening provided by the other shells. Hence the impedance Z is reduced in MWNTs, and the LL exponent α should be small compared to SWNTs. The physics behind the anomaly is different in LL and EQFT cases. In EQFT the power law arises as the tunneling electron needs to exchange energy with the external transmission line to overcome the potential barrier, while in LL model there are no single-particle states for the electron to tunnel into. Difference between the predictions of the two models arises at high voltages, where the Luttinger liquid theory fails to include the Coulomb offset observed in [P5], and therefore better description is given by the EQFT.

5 Single-electron devices and noise

The construction and characterization of nanotube-SETs is described in publications [P6-P8]. A nanotube can make a nice island, basically because it is small enough to have quite tiny capacitance, which is difficult to reach via lithographic techniques. Moreover, it is a good conductor. In practice, a nanotube may or may not give a practical or even operational device: 1) there should not be any breaks in the nanotube, which lead to splitting of the island into two or more sections, and 2) the RC time constant of the nanotube should not be so large that it leads to suppression of gate modulation. The gate voltage characteristics of devices constructed using CVD tubes do not show any regular Coulomb oscillations (see Fig. 5 in [P6]) and, hence, they are useless as electrometers. Arc-discharge tube devices, on the other hand, work quite well [P7,P8]. A good length for the nanotube is on the order of 1 μm or less. Otherwise, the stray capacitance starts to suppress the charging energy [89].

From the practical point of view, an important consideration is the noise level of the devices, which limits their charge sensitivity. In metallic single-electron devices, the low frequency operation is plagued by the $1/f$ noise, which typically arises from either charge fluctuations in the nearby dielectric materials, or resistance fluctuations of the tunnel junctions [90]. Background charge fluctuations in carbon nanotube SETs were considered in publications [P7] and [P8]. The topic of [P9] is $1/f$ type of noise outside the Coulomb blockade regime, which is not arising from background charges.

In [P7], a nanotube-SET was made of two crossing nanotubes, by evaporating the contacts on top of the nanotubes. The lower tube acted as the island. Because it turned out that the electrical contact between the two tubes was very bad, it was possible to operate the upper tube as a near-by gate electrode, which provided a larger gate capacitance than the lithographically manufactured side gate located relatively far from the nanotubes. The characteristic diamond pattern, as seen in Fig. 5.1(a), is quite regular. The

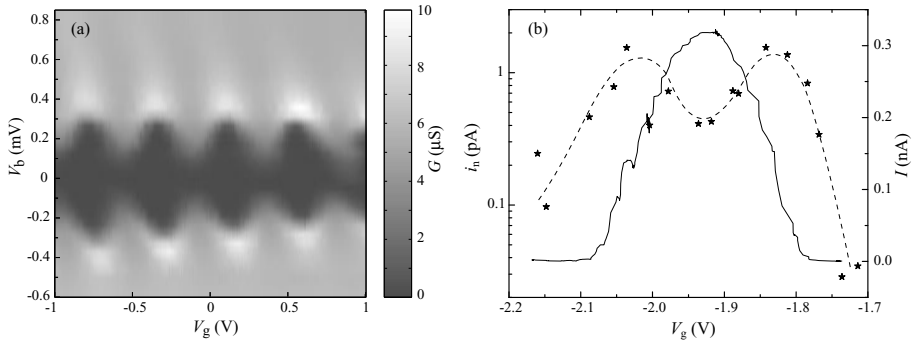

Figure 5.1: (a) Grayscale plot of nanotube SET conductance as a function of gate and bias voltages. (b) The modulation of current noise (stars, left axis) and current (solid line, right axis) vs gate voltage. The dashed line is a guide to the eyes. The noise has maxima at the maxima of the transconductance dI/dV_g. The noise minima corresponding to the minimum of current are deeper than the local minimum at maximum of current.

most notable difference between the characteristics of our nanotube device and typical metallic one is that the gap (see Fig. 5.1(a)) is not fully closed at any value of V_g. The standard analysis yields junction capacitances $C_1 = 220$ aF and $C_2 = 320$ aF. This analysis yields the total capacitance (including any self-capacitance), as opposed to the high-voltage tails analysis of [P5], which gives an estimate for the junction capacitance only ($C_T = 110$ aF), and the self-capacitance is treated as a part of the electromagnetic environment of the junction.

The current noise, recorded over one period of modulation as a function of V_g, shows the highest values around the maxima of dI/dV_g, indicating that the background charge fluctuations contribute to the noise (Fig. 5.1(b)). In addition to the gate dependent part of the $1/f$ noise, there is another contribution, which increases as a function of the current, and hence the noise is considerably higher close to the maximum of current than it is near the minima, even though the charge sensitivity is zero in both cases.

In [P8], the nanotube-SET was constructed in the reverse order: the electrodes were done first and AFM manipulation was employed to move the nanotube to the desired location over the electrodes, fully detached from the SiO_2 substrate. The sample was heat treated at 700 °C, resulting in slight sinking of the nanotube into the gold electrodes. The final resistance was quite low for a SET, and the characteristics show signs of quantum-dot-like behavior. In this sample, charge noise of 6×10^{-6} e/$\sqrt{\text{Hz}}$ at $f = 45$ Hz was measured, which is comparable to best metallic devices [91]. In [P7], the

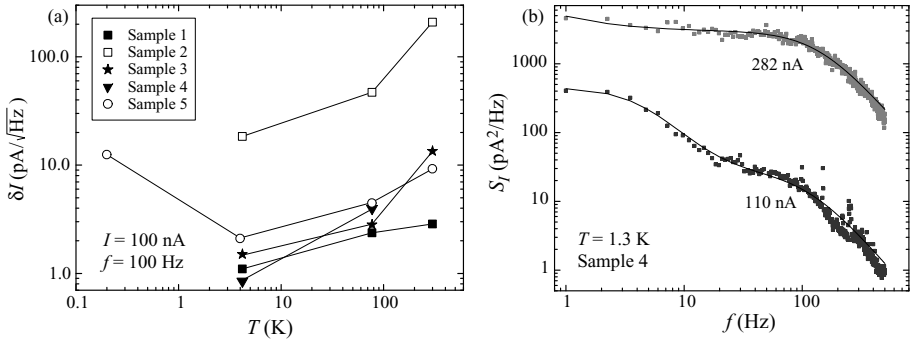

Figure 5.2: (a) The noise levels of several MWNT samples, characterized at a few different temperatures. (b) Typically the power spectra observed at 4.2 K and below show contributions of individual two-level fluctuators. The sample spectra were recorded at 1.3 K. The solid lines are obtained by fitting Eq. (5.1) with a small overall $1/f$ background.

noise level was found not exceptional but rather typical for a SET. Charge noise is reduced when the island is further away from any dielectric material such as the substrate [90].

The current dependent $1/f$ noise, already observed in [P7], was further studied in [P9]. The samples were prepared with the nanotubes on top of the electrodes, which is supposed to be less susceptible to charge fluctuation noise. In analogy to the usual oxide tunnel junction devices, resistance fluctuations of the contacts are a likely origin of $1/f$ noise. Another possibility is that the resistance of the nanotube itself fluctuates. While in metallic devices the tunnel barrier is well-defined, in carbon nanotubes the microscopic structure of the tunnel barrier is not really known. In the light of the accidental nature of the tunnel junctions, it is not that surprising that the quality of these contacts varies a lot from sample to sample and they may be extremely noisy. The current noise of several samples as a function of temperature is shown in Fig. 5.2(a) [P9]. The range of noise levels found in the samples is wide. Notably, the noisiest sample has one very short contact and is also partly touching the substrate. The noise power was observed to decrease by a factor 10-100 going from room temperature to 4.2 K.

At low temperatures, the current noise spectra (Fig. 5.2(b)) were no longer of simple $1/f^{\alpha}$-type, but were observed to consist of a sum of Lorentzian line shapes

$$S_I = I^2 \sum_i \frac{S_{\mathrm{L}}^{(i)} \tau_i}{1 + 4\pi^2 \tau_i^2 f^2}, \tag{5.1}$$

where each Lorentzian is characterized by an effective lifetime τ_i and an amplitude $S_{\mathrm{L}}^{(i)}$. The details are different for each sample and asymmetric with respect to the bias direction. The power spectrum of Eq. (5.1) arises from a noise signal which shows fluctuations between two current states. The analysis in [P9] has shown that these fluctuations can be on the order of $\Delta R \sim 1\ \mathrm{k}\Omega$, which is not likely to arise from the nanotube itself, but suggests that the contacts most likely dominate the measured noise, and the intrinsic noise behavior of the nanotube is not observed.

6 Discussion

In this Thesis, electronic transport in CVD grown carbon nanotubes is characterized in detail, and tunneling between metallic electrodes and carbon nanotubes is studied in both disordered and relatively clean samples. The disordered regime has not been studied in this extent before.

The separation of the intrinsic nanotube properties from tunneling phenomena originating at the contacts is tricky in good-quality (ballistic) nanotubes, as well as in disordered nanotubes. In this Thesis work, the best effort has been made to study the physics of intrinsic and contact-dominated transport separately. Nevertheless, in transport studies even a few kilo-ohms of resistance in contacts will give rise to tunneling effects of strong tunneling character, and in the opposing case of the high resistance tunnel junctions, the temperature-dependent change of the nanotube resistance cannot be completely eliminated. Four-lead measurements are ineffective in solving this issue. Despite these difficulties, the main characteristics of each case have been observed and analyzed, and the inherent complexity of the system only affects the accuracy of the analysis.

The work in this Thesis covers most aspects of the effect of strong disorder on electrical transport in nanotubes. The pointers that indicate that strong disorder exists include (1) smooth G–V characteristics at low temperatures, (2) weak negative magnetoresistance, (3) logarithmic (ohmic contacts) or $\exp(-\sqrt{T_0/T})$ (tunnel junctions) suppression of conductivity, and, of course, (4) very high 4-lead resistivity. Observation of these signs in any particular batch of nanotubes should be taken as a sign that the level of disorder is high.

The tunneling conductivity in good quality samples was measured and analyzed in terms of the environmental quantum fluctuation theory. The conclusions have been later[1] confirmed by several other groups [49, 51, 52], and they can be considered as well-established. The measurements on disordered samples, on the other hand, possess some novelty and constitute a

[1]The manuscript of [P5] was originally submitted to Phys. Rev. Lett. on Nov. 27, 2000.

way to experimentally verify the recent theoretical calculation beyond first order [78, 79], which have been tested experimentally to a lesser degree [77].

Nanotube-SETs constructed using nanotubes of varying quality and different geometries were studied. Both poor quality nanotubes and contacts can cause quite a lot of trouble when attempting to construct nanotube devices. In nanotube SETs, the ill-defined, accidental nature of the tunnel junctions can give rise to a large amount of $1/f$ noise at audio frequencies and some unexpected contact phenomena. An initial attempt to construct better defined tunnel junctions was made, using traditional aluminum oxide barrier, but no improvement was found.

Generally, considerable amount of research effort has been invested in the study of electrical transport in multiwalled carbon nanotubes. Even though the results of different experiments vary, which may seem controversial at first glance, in the light of the widely ranging quality of the material it is quite understandable that transport experiments reflect this variety. To put the potential of the nanotube material into use, it is quite important that the quality of the nanotubes is known and good enough for the purpose at hand. Also the manufacture of the samples has to be controlled and reliable, so that repeatable result can be obtained.

References

[1] S. Iijima, *Helical microtubules of graphitic carbon*, Nature **354**, 56 (1991).

[2] S. Datta, *Electronic transport in mesoscopic systems* (Cambridge university press, Cambridge, 1997).

[3] G. Bergmann, *Weak localization in thin films*, Phys. Rep. **107**, 1 (1984).

[4] B. L. Al'tshuler, A. G. Aronov, M. E. Gershenson, and Y. V. Sharvin, *Quantum effects in disordered metal films*, Sov. Sci. Rev. A Phys. **9**, 223 (1987).

[5] B. L. Altshuler and A. G. Aronov, in *Electron-Electron Interaction in Disordered Systems*, edited by A. L. Efros and M. Pollak (Elsevier science publishers B. V., Amsterdam, 1985), p. 1.

[6] M. P. A. Fisher and L. I. Glazman, in *Mesoscopic electron transport*, Vol. 345 of *NATO ASI Series E: Applied sciences*, edited by L. L. Sohn, L. P. Kouwenhoven, and G. Schön (Kluwer academic publishers, Dordrecht, 1997), p. 331.

[7] B. L. Al'tshuler, A. G. Aronov, and A. Y. Zyuzin, *Size effects in disordered conductors*, Sov. Phys. JETP **59**, 415 (1984).

[8] M. Bockrath, D. H. Cobden, P. L. McEuen, N. G. Chopra, A. Zettl, A. Thess, and R. E. Smalley, *Single-electron transport in ropes of carbon nanotubes*, Science **275**, 1922 (1997).

[9] S. J. Tans, M. H. Devoret, H. Dai, A. Thess, R. E. Smalley, L. J. Geerligs, and C. Dekker, *Individual single-wall carbon nanotubes as quantum wires*, Nature **386**, 474 (1997).

[10] L. Roschier, J. Penttilä, M. Martin, P. Hakonen, M. Paalanen, U. Tapper, E. I. Kauppinen, C. Journet, and P. Bernier, *Single-electron transistor made of multiwalled carbon nanotube using scanning probe manipulation*, Appl. Phys. Lett. **75**, 728 (1999).

[11] N. Hamada, S. Sawada, and A. Oshiyama, *New one-dimensional conductors: Graphitic microtubules*, Phys. Rev. Lett. **68**, 1579 (1992).

[12] R. Saito, G. Dresselhaus, and M. S. Dresselhaus, *Physical Properties of Carbon Nanotubes* (Imperial College Press, London, 1998).

[13] A. Koshio, M. Yudasaka, and S. Iijima, *Metal-free production of high-quality multi-wall carbon nanotubes, in which the innermost nanotubes have a diameter of 0.4 nm*, Chem. Phys. Lett. **356**, 595 (2002).

[14] K. Hernadi, A. Fonseca, J. B. Nagy, D. Bernaerts, A. Fudala, and A. A. Lucas, *Catalytic sythesis of carbon nanotubes using zeolite support*, Zeolites **17**, 416 (1996).

[15] M. Ahlskog, E. Seynaeve, R. J. M. Vullers, C. V. Haesendonck, A. Fonseca, K. Hernadi, and J. B. Nagy, *Ring formation from catalytically synthesized carbon nanotubes*, Chem. Phys. Lett. **300**, 202 (1999).

[16] S. Amelinckx, X. B. Zhang, D. Bernaerts, X. F. Zhang, V. Ivanov, and J. B. Nagy, *A formation mechanism for catalytically grown helix-shaped graphite nanotubes*, Science **265**, 635 (1994).

[17] J.-P. Salvetat, A. J. Kulik, J.-M. Bonard, G. A. D. Briggs, T. Stöckli, K. Méténier, S. Bonnamy, F. Béguin, N. A. Burnham, and L. Forró, *Elastic Modulus of Ordered and Disordered Multiwalled Carbon Nanotubes*, Adv. Mater. **11**, 161 (1999).

[18] L. Langer, V. Bayot, E. Grivei, J.-P. Issi, J. P. Heremans, C. H. Olk, L. Stockman, C. V. Haesendonck, and Y. Bruynseraede, *Quantum Transport in a Multiwalled Carbon Nanotube*, Phys. Rev. Lett. **76**, 479 (1996).

[19] A. Y. Kasumov, I. I. Khodos, P. M. Ajayan, and C. Colliex, *Electrical resistance of a single carbon nanotube*, Europhys. Lett. **34**, 429 (1996).

[20] H. Dai, E. W. Wong, and C. M. Lieber, *Probing Electrical Transport in Nanomaterials: Conductivity of Individual Carbon nanotubes*, Science **272**, 523 (1996).

[21] T. W. Ebbesen, H. J. Lezec, H. Hiura, J. W. Bennett, H. F. Ghaemi, and T. Thio, *Electrical conductivity of individual carbon nanotubes*, Nature **382**, 54 (1996).

[22] A. Y. Kasumov, H. Bouchiat, B. Reulet, O. Stephan, I. I. Khodos, Y. B. Gorbatov, and C. Colliex, *Conductivity and atomic structure of isolated multiwalled carbon nanotubes*, Europhys. Lett. **43**, 89 (1998).

[23] A. Fujiwara, K. Tomiyama, H. Suematsu, M. Yumura, and K. Uchida, *Quantum interference of electrons in multiwall carbon nanotubes*, Phys. Rev. B **60**, 13492 (1999).

[24] A. Bachtold, C. Strunk, J.-P. Salvetat, J.-M. Bonard, L. Forró, T. Nussbaumer, and C. Schönenberger, *Aharonov-Bohm oscillations in carbon nanotubes*, Nature **397**, 673 (1999).

[25] C. Schönenberger, A. Bachtold, C. Strunk, J.-P. Salvetat, and L. Forró, *Interference and Interactions in multi-wall carbon nanotubes*, Appl. Phys. A **69**, 283 (1999).

[26] S. Frank, P. Poncharal, Z. L. Wang, and W. A. de Heer, *Carbon Nanotube Quantum Resistors*, Science **280**, 1744 (1998).

[27] P. Poncharal, C. Berger, Y. Yi, Z. L. Wang, and W. A. de Heer, *Room temperature ballistic conduction in carbon nanotubes*, J. Phys. Chem. B **106**, 12104 (2002).

[28] A. Bachtold, M. S. Fuhrer, S. Plyasunov, M. Forero, E. H. Anderson, A. Zettl, and P. L. McEuen, *Scanned Probe Microscopy of Electronic Transport in Carbon Nanotubes*, Phys. Rev. Lett. **84**, 6082 (2000).

[29] S. J. Tans, A. R. M. Verschueren, and C. Dekker, *Room-temperature transistor based on a single carbon nanotube*, Nature **393**, 49 (1998).

[30] A. Javey, M. Shim, and H. Dai, *Electrical properties and devices of large-diameter single-walled carbon nanotubes*, Appl. Phys. Lett. **80**, 1064 (2002).

[31] A. Javey, J. Guo, Q. Wang, M. Lundstrom, and H. Dai, *Ballistic carbon nanotube field-effect transistors*, Nature **424**, 654 (2003).

[32] D. Mann, A. Javey, J. Kong, Q. Wang, and H. Dai, *Ballistic transport in metallic nanotubes with reliable Pd ohmic contacts*, Nano Lett. **3**, 1541 (2003).

[33] J. W. G. Wildöer, L. C. Venema, A. G. Rinzler, R. E. Smalley, and C. Dekker, *Electric structure of atomically resolved carbon nanotubes*, Nature **391**, 59 (1998).

[34] J. Nygård, D. H. Cobden, and P. E. Lindelof, *Kondo physics in carbon nanotubes*, Nature **408**, 342 (2000).

[35] D. H. Cobden and J. Nygård, *Shell filling in closed single-wall carbon nanotube quantum dots*, Phys. Rev. Lett. **89**, 046803 (2002).

[36] M. Bockrath, D. H. Cobden, J. Lu, A. G. Rinzler, R. E. Smalley, L. Balents, and P. L. McEuen, *Luttinger-liquid behaviour in carbon nanotubes*, Nature **397**, 598 (1999).

[37] W. Liang, M. Bockrath, D. Bozovic, J. H. Hafner, M. Tinkham, and H. Park, *Fabry-Perot interference in a nanotube electron waveguide*, Nature **411**, 665 (2001).

[38] J. Kong, E. Wenilmez, T. W. Tombler, W. Kim, H. Dai, R. B. Laughlin, L. Liu, C. S. Jayanthi, and S. Y. Wu, *Quantum interference and ballistic transmission in nanotube electron waveguides*, Phys. Rev. Lett. **87**, 106801 (2001).

[39] M. Kociak, A. Y. Kasumov, S. Guéron, B. Reulet, I. I. Khodos, Y. B. Gorbatov, V. T. Volkov, L. Vaccarini, and H. Bouchiat, *Superconductivity in ropes of single-walled carbon nanotubes*, Phys. Rev. Lett. **86**, 2416 (2001).

[40] M. Krüger, M. R. Buitelaar, T. Nussbaumer, C. Schönenberger, and L. Forró, *The electrochemical carbon nanotube field-effect transistor*, Appl. Phys. Lett. **78**, 1291 (2001).

[41] B. Q. Wei, R. Vajtai, and P. M. Ajayan, *Reliability and current carrying capacity of carbon nanotubes*, Appl. Phys. Lett. **79**, 1172 (2001).

[42] K. Liu, P. Avouris, R. Martel, and W. K. Hsu, *Electrical transport in doped multiwalled carbon nanotubes*, Phys. Rev. B **63**, 161404 (2001).

[43] Z. Yao, C. L. Kane, and C. Dekker, *High-field electrical transport in single-wall carbon nanotubes*, Phys. Rev. Lett. **84**, 2941 (2000).

[44] P. G. Collins, M. Hersam, M. Arnold, R. Martel, and P. Avouris, *Current Saturation and Electrical Breakdon in Multiwalled Carbon Nanotubes*, Phys. Rev. Lett. **86**, 3128 (2001).

[45] B. Bourlon, D. C. Glattli, B. Plaçais, J. M. Berroir, C. Miko, L. Forró, and A. Bachtold, *Geometrical Dependence of High-Bias Current in Multiwalled Carbon Nanotubes*, Phys. Rev. Lett. **92**, 026804 (2004).

[46] C. Berger, Y. Yi, J. Gezo, P. Poncharal, and W. A. de Heer, *Contacts, non-linear transport effects and failure in multi-walled carbon nanotubes*, New J. Phys. **5**, 158 (2003).

[47] Y.-G. Yoon, P. Delaney, and S. G. Louie, *Quantum conductance of multiwall carbon nanotubes*, Phys. Rev. B **66**, 073407 (2002).

[48] Y. X. Liang, Q. H. Li, and T. H. Wang, *Current saturation in multiwalled Carbon nanotubes by large bias*, Appl. Phys. Lett. **84**, 3379 (2004).

[49] A. Bachtold, M. de Jonge, K. Grove-Rasmussen, P. L. McEuen, M. Buitelaar, and C. Schönenberger, *Suppression of Tunneling into Multiwall Carbon Nanotubes*, Phys. Rev. Lett. **87**, 166801 (2001).

[50] E. Graugnard, P. J. de Pablo, B. Walsh, A. W. Ghosh, S. Datta, and R. Reifenberger, *Temperature dependence of the conductance of multiwalled carbon nanotubes*, Phys. Rev. B **64**, 125407 (2001).

[51] A. Kanda, K. Tsukagoshi, Y. Aoyagi, and Y. Ootuka, *Gate-Voltage Dependence of Zero-Bias Anomalies in Multiwalled Carbon Nanotubes*, Phys. Rev. Lett. **92**, 036801 (2004).

[52] W. Yi, L. Lu, H. Hu, Z. W. Pan, and S. S. Xie, *Tunneling into Multiwalled Carbon Nanotubes: Coulomb Blockade and the Fano Resonance*, Phys. Rev. Lett. **91**, 076801 (2003).

[53] A. Kanda, Y. Ootuka, K. Tsukagoshi, and Y. Aoyagi, *Electron transport in metal/multiwall carbon nanotube/metal structures (metal=Ti or Pt/Au)*, Appl. Phys. Lett. **79**, 1354 (2001).

[54] A. Kanda, K. Tsukagoshi, S. Uryu, Y. Ootuka, and Y. Aoyagi, *Resistance dependence of transport properties in metal-multiwall carbon nanotube-metal structures*, Microel. Eng. **63**, 33 (2002).

[55] M. R. Buitelaar, A. Bachtold, T. Nussbaumer, M. Iqbal, and C. Schönenberger, *Multiwall Carbon Nanotubes as Quantum Dots*, Phys. Rev. Lett. **88**, 156801 (2002).

[56] M. R. Buitelaar, T. Nussbaumer, and C. Schönenberger, *A Quantum Dot in the Kondo Regime Coupled to Superconductors*, Phys. Rev. Lett. **89**, 256801 (2002).

[57] M. Martin, L. Roschier, P. Hakonen, Ü. Parts, M. Paalanen, B. Schleicher, and E. I. Kauppinen, *Manipulation of Ag nanoparticles utilizing noncontact atomic force microscopy*, Appl. Phys. Lett. **73**, 1505 (1998).

[58] G. Binnig, C. F. Quate, and C. Gerber, *Atomic force microscope*, Phys. Rev. Lett. **56**, 930 (1986).

[59] R. Wiesendanger, *Scanning probe microscopy and spectroscopy* (Cambridge university pres, Cambridge, 1994).

[60] J.-O. Lee, C. Park, J.-J. Kim, J. Kim, J. W. Park, and K.-H. Yoo, *Formation of low-resistance ohmic contacts between carbon nanotube and metal electrodes by a rapid thermal annealing method*, Journal of Physics D: Applied Physics **33**, 1953 (2000).

[61] J. P. Pekola, K. P. Hirvi, J. P. Kauppinen, and M. A. Paalanen, *Thermometry by Arrays of Tunnel Junctions*, Phys. Rev. Lett. **73**, 2903 (1994).

[62] Lake Shore Cryotronics, 575 McCorkle Blvd. Westerville, OH 43082-8888, www.lakeshore.com.

[63] S. Hikami, A. I. Larkin, and Y. Nagaoka, *Spin-orbit interaction and magnetoresistance in the two-dimensional random system*, Prog. Theor. Phys. **63**, 707 (1980).

[64] I. L. Aleiner, B. L. Altshuler, and M. E. Gershenson, *Interaction effects and phase relaxation in disordered systems*, Waves in Random Media **9**, 201 (1999).

[65] G. Zala, B. N. Narozhny, and I. L. Aleiner, *Interaction corrections at intermediate temperatures: Longitudinal conductivity and kinetic equation*, Phys. Rev. B **64**, 214204 (2001).

[66] S. Farhangfar, R. S. Poikolainen, J. P. Pekola, D. S. Golubev, and A. D. Zaikin, *Coulomb blockade in one-dimensional arrays of high-conductance tunnel junctions*, Phys. Rev. B **63**, 075309 (2001).

[67] P. Kim, L. Shi, A. Majumdar, and P. L. McEuen, *Mesoscopic thermal transport and energy dissipation in carbon nanotubes*, Physica B **323**, 67 (2002).

[68] F. C. Wellstood, C. Urbina, and J. Clarke, *Hot-electron effects in metals*, Phys. Rev. B **49**, 5942 (1994).

[69] H. Pothier, S. Guéron, N. O. Birge, D. Esteve, and M. H. Devoret, *Energy distribution function of quasiparticles in mesoscopic wires*, Phys. Rev. Lett. **79**, 3490 (1997).

[70] V. Bayot, L. Piraux, J. P. Michenaud, and J. P. Issi, *Evidence for weak localization in the thermal conductivity of a quasi-two-dimensional electron system*, Phys. Rev. Lett. **65**, 2579 (1990).

[71] D. R. Niven and R. A. Smith, *Electron-electron interaction corrections to the thermal conductivity in disordered conductors*, Phys. Rev. B **71**, 035106 (2005).

[72] L. Lu, W. Yi, and D. L. Zhang, *3ω method for specific heat and thermal conductivity measurements*, Rev. Sci. Instr. **72**, 2996 (2001).

[73] G.-L. Ingold and Y. V. Nazarov, in *Single Charge Tunneling*, edited by H. Grabert and M. H. Devoret (Plenum Press, New York, 1992), pp. 21–107.

[74] F. Pierre, H. Pothier, P. Joyez, N. O. Birge, D. Esteve, and M. H. Devoret, *Electrodynamic Dip in the Local Density of States of a Metallic Wire*, Phys. Rev. Lett. **86**, 1590 (2001).

[75] F. Pierre, Ph.D. thesis, Université Paris 6, 2000.

[76] W. Zheng, J. R. Friedman, D. V. Averin, S. Han, and J. E. Lukens, *Observation of strong Coulomb blockade in resistively isolated tunnel junctions*, Solid State Comm. **108**, 839 (1998).

[77] V. Krstić, S. Blumentritt, J. Muster, S. Roth, and A. Rubio, *Role of disorder on transport in boron-doped multiwalled carbon nanotubes*, Phys. Rev. B **67**, 041401 (2003).

[78] J. Rollbühler and H. Grabert, *Coulomb blockade of tunneling between disordered conductors*, Phys. Rev. Lett. **87**, 126804 (2001).

[79] E. G. Mishchenko, A. V. Andreev, and L. I. Glazman, *Zero-bias anomaly in disordered wires*, Phys. Rev. Lett. **87**, 246801 (2001).

[80] P. Joyez and D. Esteve, *Single-electron tunneling at high temperature*, Phys. Rev B **56**, 1848 (1997).

[81] E. Sonin, private communication (unpublished).

[82] P. Joyez, D. Esteve, and M. H. Devoret, *How is the Coulomb blockade suppressed in high-conductance tunnel junctions?*, Phys. Rev. Lett. **80**, 1956 (1998).

[83] M. Bockrath, Ph.D. thesis, University of California, Berkeley, 1999.

[84] P. Wahlgren, P. Delsing, and D. B. Haviland, *Crossover from global to local rule for the Coulomb blockade in small tunnel junction*, Phys. Rev. B **52**, 2293 (1995).

[85] R. Egger, *Luttinger Liquid Behavior in Multiwall Carbon Nanotubes*, Phys. Rev. Lett. **83**, 5547 (1999).

[86] R. Egger and A. O. Gogolin, *Correlated transport and non-Fermi-liquid behavior in single-wall carbon nanotubes*, Eur. Phys. J. B **3**, 281 (1998).

[87] M. Zamkov, N. Woody, B. Shan, Z. Chang, and P. Richard, *Lifetime of charge carriers in multiwalled nanotubes*, Phys. Rev. Lett. **94**, 056803 (2005).

[88] E. B. Sonin, *Tunneling into 1D and Quasi-1D Conductors and Luttinger-liquid Behavior*, J. Low Temp. Phys. **124**, 321 (2001).

[89] J. G. Lu, J. M. Hergenrother, and M. Tinkham, *Effect of island length on the Coulomb modulation in single-electron transistors*, Phys. Rev. B **57**, 4591 (1998).

[90] V. A. Krupenin, D. E. Presnov, M. N. Savvateev, H. Scherer, A. B. Zorin, and J. Niemeyer, *Noise in Al single electron transistors of stacked design*, J. Appl. Phys. **84**, 3212 (1998).

[91] V. A. Krupenin, D. E. Presnov, A. B. Zorin, and J. Niemeyer, *Aluminum single electron transistors with islands isolated from the substrate*, J. Low Temp. Phys. **118**, 287 (2000).